Results in Engineering 30 (2026) 111334

Contents lists available at ScienceDirect

Results in Engineering

journal homepage: www.sciencedirect.com/journal/results-in-engineering

5E assessments and economic–financial viability of an innovative direct-contact photovoltaic thermal system: Experimental and numerical study

Yassine El Alami [a,*], Jaouad El Gharfaoui [a], Zineb Hekss [b], Charaf Hajjaj [a], Fatima Chanaa [c], Elhadi Baghaz [a], Mohammed Ghazal [d], Adnan Ibrahim [e,*]

[a] Laboratory of Electronics, Instrumentation and Energetic, Faculty of Sciences, Chouaïb Doukkali University, El Jadida, Morocco
[b] High School of Technology of Sidi Bennour Chouaïb Doukkali University of El Jadida, Morocco
[c] Systems Control, Pilotage and Supervision Team, Engineering Sciences and Professions Laboratory, ENSAM, Moulay Ismaïl University, Meknes, Morocco
[d] Electrical, Computer and Biomedical Engineering Department, Abu Dhabi University, Abu Dhabi, PO Box 59911, United Arab Emirates
[e] Solar Energy Research Institute, Universiti Kebangsaan Malaysia, 43600, Bangi, Selangor, Malaysia

ARTICLE INFO

Keywords:
Photovoltaic-thermal system
Direct heat exchanger
Energy and economic analysis
Exergy analysis
Levelized cost of electricity (LCOE)

ABSTRACT

Photovoltaic-thermal systems (PVT-S) still have several limitations, such as excess weight, expansion constraints on the absorber plate, and insufficient cooling efficiency. To address these issues, this study proposes a new PVT-S configuration incorporating a heat exchanger that allows direct contact between the heat transfer fluid and the rear surface of the photovoltaic (PV) module, and compares its summer performance with that of a reference PV module (PV-M). In order to predict and optimize performance, a three-dimensional model was developed using COMSOL Multiphysics and validated experimentally under the climatic conditions of El Jadida. The results were analyzed in terms of energy and exergy performance and temperature distribution. In addition, the study includes sustainability indicators, an annual and environmental assessment, exergy destruction, entropy generation, and an economic analysis taking into account the payback time (PBT) and the levelized cost of electricity (LCOE). The new PVT-S achieves a maximum thermal efficiency of 76.885% and an average exergy efficiency of 15.313%, with an exergy destruction of 924.712 W and an entropy generation of 3.020 W/ °C. It has an average sustainability index of 1.18084, an average improvement potential (IP) of 783.106 W, an average Waste Exergy Ratio (WER) of 0.84837, and an average ecological exergy indicator (EcEI) of -0.69373. The total annual energy is 2837.86 kWh, reducing CO_2 emissions to 7.922 t/year, compared to 534.81 kWh and 2.920 t/year for the reference PV. The investment cost is 1870.97 $, with a PBT of 4.709 years and an LCOE of 0.11271 $/kWh.

1. Introduction

The energy transition is getting critical due to the ever-growing consumption and the rising pressure on the use of fossil fuel resources [1]. Further consumption of fossil fuels is exacerbating the situation regarding global warming and CO_2 emissions, which is why a shift towards renewable and sustainable sources of energy is an urgent requirement [2]. Solar energy is one of such sources that are the most abundant and can provide a significant volume of energy that can be transformed into electricity with the help of PV- Ms [3–5]. These modules are very flexible about to installation since they can be mounted on buildings, urban infrastructure, or be mounted as autonomous systems. However, the performance of PV-Ms is still low and is extremely influenced by their temperature of operation [6,7]. Moreover, an increase in cell temperature causes a significant decrease in electrical efficiency (EEF), and an increase in cell temperature by correct cooling can increase it by 10 to 25% [8]. In this regard, low-cost, low--energy-consumption, and efficient thermal-management systems are needed to maximize electricity generation. It is within this context that PVT-Ss have been created [9–11]. These systems allow the production of electricity and heat, incorporating sensors on the rear of PV-Ms, and thus lowering their temperatures and enhancing the total output [12,13]. Over the past decades, PVT-S architecture has been profoundly evolving, shifting its primitive designs to sophisticated assemblies that combine synergistically passive and active cooling schemes, rational material

* Corresponding authors.
E-mail addresses: yassineelalami97@gmail.com (Y. El Alami), iadnan@ukm.edu.my (A. Ibrahim).

https://doi.org/10.1016/j.rineng.2026.111334
Received 24 December 2025; Received in revised form 8 May 2026; Accepted 31 May 2026
Available online 1 June 2026

Nomenclature

Abbreviations

PBT	Payback time
PV-M	Photovoltaic module
EcEI	Ecological efficiency index
PVT-S	Photovoltaic thermal system
EVA	Ethylene vinyl acetate
IP	Improvement potential
EEF	Electrical efficiency
LCOE	Levelized cost of electricity
FF	Form factor
TEF	Thermal efficiency
SI	Sustainability index
WER	waste exergy ratio
FEM	Finite element method
MFRT ($\dot{m}_f$)	Mass Flow rate

Parameters

$\varnothing_{CO2}$	Annual CO_2 reduction (tCO_2/year)
T_g	Glass temperature (°°C)
k	Thermal conductivity (W/m.K)
Z_{CO_2}	Environmental cost ($)
T_{ted}	Tedlar temperature (°°C)
$\dot{E}_{sun,in}$	Received energy (W)
P_{CO_2}	Average carbon price
V_{oc}	Open-circuit voltage
$\dot{Q}_u$	Average energy gain
$\dot{E}_{th}$	Thermal energy (W)
Ts	Surface temperature, (°°C)
T_g	Glass temperature (°°C)
$\dot{X}_{th}$	Thermal exergy (W)
A_{PV}	PV area (m^2)
i	Discount rate
T_{out}	Output water temperature (°°C)
u, v, w	Velocity components (m/s)
n	Surface normal
d_g	Degradation rate (%)
P_c	Packing factor (%)
$\dot{X}_{el}$	Electrical exergy (W)
G_t	Annual solar radiation (W/m^2)
V_{oc}	Open-circuit voltage
C_p	Specific heat (J/Kg K)
$T_{in,f}$	Inlet temperature (°°C)
C_0	Initial cost
$\dot{X}_{sun}$	Exergy solar radiation
$\dot{X}_{des}$	Exergy destruction
$\dot{E}_{el}$	Electrical power (W)
$M_{t,el}$	Annual electricity savings
A_t	Annual maintenance
T_c	Solar cell temperature (°°C)
$\dot{S}_{gen}$	Entropy generation
I_{sc}	Short-circuit current
$T_{out,f}$	Outlet temperature (°°C)
q	Heat flow vector

Greek Symbols

η_{el}	Electrical efficiency (%)
ε_{el}	Exergy efficiency (electrical) (%)
ε_{PVT}	Exergy efficiency (total) (%)
ρ	Density (Kg/m^3)
η_{th}	Thermal efficiency (%)
η_{el}	Electrical efficiency (%)

optimization, and novel geometrical designs. This steady enhancement is aggressively pursued with the twofold purpose of enhancing energy conversion efficiency as well as maintaining an astonishing compact size, and at the same time, is protective of the economic sustainability of the system.

The literature has analyzed several concepts and geometry settings to make PVT systems optimize their performance. The geometry of the thermal collectors, the nature and placement of the fins, and the design of the fluid circulation channels are the most common subjects of research in which investigators are interested, and all have an impact on the total energy yield. A new PVT system in which the collector is constructed by using perforated twisted ribbons to cool the modules was assessed by Göksu et al. [14]. In this design, they stated that the EEF was 12.8% and the thermal efficiency (TEF) was 40.6%; this was reported to bring both the surface temperature of the panel decreasing and high key performance metrics in comparison to the conventional architecture. Zaini et al. [15] have explored a PVT-S with an active water-cooling system to reduce the temperatures of panels. The cooling system also enhanced the electricity production by 16.5%, and the resultant net energy efficiency of 83.3% exceeded the standard PVT-S performance and enhanced convective heat transfer. The PVT-S introduced by Ahmed et al. [16] is an innovative collector with helical ribbons and petal-shaped surface, the use of phase-change materials, and silicon carbide nanofluids. The resultant design reported an exergy efficiency of 11.86%, maximum overall energy efficiency of 97.34%, and minimum cost factor of 0.820, which shows a high level of performance and economic feasibility. In a study by Parach et al. [17] experimented with a PVT-S with the inclusion of PCM was experimented using a series of different rectangular fin absorber designs. The arrangement with the ratio of fin to channel height of 0.9 provided the most beneficial results, which suppressed the panel temperature and enhanced the melting of PCM, and hence a maximum EEF factor of 13.5% of the panel. Beltrán et al. [18] developed an exchange of a PVT-S combined with a heat pump that consists of a corrugated polycarbonate absorber with fins, which works under forced convection. This corrugated wall design increases the total heat-transfer coefficient by about 15–30%, which translates to a reduction of 6–10 °C in the center of the surface of the PV-M. This results in a relative 4–7% increase in the EEF of the module compared to the traditional flat-plate and tube model. Al-Karboly et al. [19] examined a new PVT, which combines a bidirectional twisted-ribbon absorber with nanostructured PCMs and nanofluids based on water with silicon carbide particles. They find that the counter-clockwise twisted-ribbon design, together with Nano-PCM, and 0.5% nanofluid concentration, achieves a total efficiency of 96.97%, including 11.26% electricity and 85.71% heat, which is 38% higher than the EEF of traditional PV systems. An investigation for a new type of PVT-S using plastic capillary mats as thermal heat exchangers was carried out by Wei et al. [20]. This low-cost design improves the recovery of heat and makes installation processes easier. The thermal performance reaches a peak efficiency of 33% and an efficiency of 52.8%, and the electrical gain is about 2.7% compared to a traditional PV-M. In addition, heat production cost is quite low, with a range of 0.010 to 0.013 USD/kWh. Perwez et al. [21] examined a new PVT-S design in the form of a relief-channel heat exchanger that was decorated with small spherical protrusions. This setup gave a 16.76% enhancement on the EEF and a maximum of 134.84 Nusselt number, thus maximizing heat transfer with a reasonable fluid circulation. Jha et al. [22] investigated another PVT-S setup that uses a trapezoidal plate exchanger. This setup had the absorber bringing the temperature of the PV-M down by 2.8 °C and the outlet temperature up by 1.9 °C over a standard flat-plate unit.

Also, the trapezoidal exchanger increased annual energy output by 8.7% and exergy recovery by 8.4% at the same time, reducing energy PBT and increasing yearly CO_2 emission reduction. Alnakeeb et al. [23] studied a new PVT-S with a trapezoidal innertube heat exchanger in series with a phase-change material. This design achieved improved values of heat transfer and overall system efficiency to 70.1% at an aspect ratio of 2 and a tube height of 9 mm. Raad et al. [24] investigated a PVT-S using a jet-water impingement exchanger to cool PV-Ms; the design achieved a peak annual energy recovery of 1354 kWh per module, savings of 582 USD, and a 785 kg CO_2 reduction in comparison to the conventional evaporative cooling strategies. Maseer et al. [25] studied an experimental PVT-S using semi-circular absorber tubes as a heat exchanger, combined with nanoparticle-enhanced phase change material (NPCM). The results show that the PVT-S using both nanofluid and NPCM achieves the best performance, with TEF of 78.99%, EEF of 12.70%, and overall efficiency of 91.83%, while reducing the surface temperature by approximately 35%. Table 1 summarizes other studies that have examined various geometric configurations of PVT-Ss, highlighting the types of collectors, channel or fin arrangements, and their effects on thermal and electrical performance.

Over the past few decades, PVT-Ss have attracted growing interest due to their ability to combine electrical and thermal production in a limited space, offering considerable potential for improving the overall energy efficiency of solar installations. Despite the many configurations developed, as shown in the analysis above, several major shortcomings remain in the thermal management of these systems. The majority of designs still rely on conventional flat plate heat exchangers, such as coils or sheet-and-tube systems, which cause significant temperature variations and can accelerate the aging of PV cells. In many configurations, an absorber plate is interposed between the PV-M and the fluid circulation tubes, limiting heat transfer, increasing the weight of the system, and sometimes causing problems with thermal expansion or air bubble formation. Furthermore, none of the studies have focused on the design of an exchanger that could be used to enable direct interaction between the heat transfer fluid and the rear of the PV-M, which is a prospective source of innovation. Finally, most studies have been limited to numerical analyses without experimental validation, which hinders the practical generalization of the results obtained and the reliability of the claimed performance.

To surmount the limitations identified in previous studies, this study proposes and analyzes an innovative PVT-S configuration that incorporates a heat exchanger allowing direct contact between the heat transfer fluid and the rear surface of the PV module. The main innovation of this design lies in the elimination of the conventional absorber plate, commonly used in traditional PVT-Ss, which represents a breakthrough in design. This approach simplifies the system's structure, reduces its mass, and limits the mechanical and thermal stresses associated with the expansion of this component, while improving direct heat transfer conditions. The proposed configuration is analyzed using detailed three-dimensional modeling in COMSOL Multiphysics and then experimentally validated under real-world conditions in the city of El Jadida. The performance analysis goes beyond conventional approaches by combining energy and exergy balances with an in-depth study of the module's internal thermal behavior, compared to a reference PV configuration. Furthermore, a sustainability assessment is conducted using several advanced indicators, including the Waste Exergy Ratio, the improvement potential, the ecological efficiency index, and the overall sustainability index, as well as an analysis of irreversibilities via exergy destruction and entropy generation. An annual analysis of energy production, coupled with an environmental assessment, is also performed to evaluate the system's overall performance over a full cycle. Finally, an economic study is conducted to estimate the PBT and the LCOE, in order to demonstrate the technical and economic viability of the proposed PVT-S configuration.

Table 1
Summary of studies on various geometric designs of PVT-Ss.

References/ Years	Type of study	Years	Absorber configuration	Major outcomes
Umam et al. [26]	Experimental	2023	Spiral and serpentine thermal collector	The spiral and serpentine collector lowered the module temperature by 5.6 °C and increased EEF by 0.53%, while insulation improved TEF by up to 18.26%.
Sachit et al. [27]	Numerical	2019	Serpentine-direct	The temperature of the cells increases with irradiation and decreases with mass flow rate. Under optimal conditions (900 W/m², 0.06 kg/s), the direct serpentine design achieves 53% TEF and 14.3% EEF, surpassing the conventional serpentine design.
Zhang et al. [28]	Experimental	2024	T-shaped evaporator heat exchanger	Panel cooling from 8.5 to 13 °C, instantaneous power increases up to 56.6%, total production gain 9.3–14.5%, efficiency 21.5–22.6%, with annual savings of up to 386.5 yuan.
Radhi et al. [29]	Experimental	2025	A micro-fin tube having a square spring and twisted tape design.	The cell temperature drops from 77.8 to 35.7 °C, EEF increases by 39%, and maximum thermal and electrical efficiencies reach 86.5% and 13.17%, with a power output of 24.44 W.
Kazem et al. [30]	Numerical and experimental	2020	web, direct, and spiral absorbers	PVT-Ss reduced cell temperature by at least 3 °C, thereby improving voltage, current, and power. The spiral flow system performed best with 17.7 V, 2.89 A, and 51.3 W, and an overall efficiency of 35%, higher than web (18.5%) and direct (28%) systems and conventional PV (7.8%).
Aghakhani et al. [31]	Numerical	2022	Serpentine tube	The best conditions for cooling and heat removal are between 0.68 and 2.5 L/min, depending on the criterion considered. EEF can reach 14.8%, while thermal and overall efficiency reach 79.1% and 92%.

(continued on next page)

Table 1 (*continued*)

References/ Years	Type of study	Years	Absorber configuration	Major outcomes
Shahsavar [32]	Experimental	2021	Sinusoidal serpentine	The combination of the sinusoidal tube and nanofluid significantly improves energy and exergy performance compared to PVT-S, with the best performance obtained at 2% nanofluid, 80 kg/h, amplitude 5 mm, and wavelength 60 mm.
Ali et al. [33]	Numerical	2024	Serpentine dual-tube	The best performance is achieved with 32 cooling loops. The unidirectional dual-tube system increases EEF and net power by approximately 10%, while the opposite dual-tube system offers slightly lower gains but reduces the maximum panel temperature, thereby extending its service life.
Madadi et Arani [34].	Experimental	2025	Flat heat sinks featuring serpentine tubes and paraffin Wax	The flat plate heat exchanger with nanofluids lowered the panel temperature, with graphene/water being the most effective. Increasing the flow rate and concentration improved heat transfer.
Alqatamin et al. [35]	Numerical	2025	Perforated V-shaped fins are incorporated in the channel structure	The perforated V-shaped fins reduced cell temperature by 31.27% and increased EEF by 18.79%, while improving energy and exergy performance by 20–40%.
Yu et al. [36]	Numerical	2021	Channels with periodic grooves	The addition of enlarged grooves in parallel channels improved heat transfer by lowering the average module temperature by approximately 4 K, with maximum flow resistance for rectangular grooves.
Nasrin et al. [37]	Numerical and experimental	2018	Serpentine tube	Water cooling improves PV performance by 9.2%; the use of nanofluid further increases thermal performance by approximately 4% (numerical) and 3.67% (experimental). The overall efficiency of the PVT-S at 1000 W/m² reaches 89.2% (numerical) and 87.65% (experimental).
Zhang et al. [38]	Numerical	2025	Absorber equipped with a multi-stage V-shaped turbulator	PVT-S which has a multi stage V-shaped turbulator enhances EEF by 9 to 12% and provides overall efficiency of >65%. The best turbulator parameters are $\beta = 61.1^{\circ}$, $\alpha = 60^{\circ}$ and D = 0 mm that is the best heat transfer and best system performance.
Satpute et al. [39]	Numerical and experimental	2025	Circular and rectangular spiral absorber	The rectangular spiral absorber has the highest performance and a maximized EEF of 14.32% and thermal recovery of 63.56% which is better compared to the circular spiral absorber as well as PV system without absorber.
Hossain et al. [40]	Experimental	2019	Parallel serpentine tube	The heat exchanger achieved a maximum heat flux of 420 W and a TEF of 76.58%, with heat loss limited to 5%.
Hosouli et al. [41]	Numerical	2024	H-pattern absorber design	The optimal configuration (2 mm cavities) reduces thermal expansion by 20% and improves thermal, electrical, and overall performance by 10%, 2%, and 8%, respectively, thereby limiting the risk of cell cracking.
Zhang et al. [42]	Numerical	2021	leaf-shaped biomimetic heat exchanger	The PVT-S, with its newly developed leaf-shaped biomimetic heat exchanger, not only provides superior cooling capability reducing the average temperature of the cell by 5.31 °C but also reduced the pressure drop by about half and increased the efficiency of the PVT-S as a whole by 4.36 °C compared to the traditional PVT-Ss.

(continued on next page)

Table 1 (*continued*)

References/ Years	Type of study	Years	Absorber configuration	Major outcomes
Ajel et al. [43]	Numerical and experimental	2023	Flat open-flow manifold with integrated fins	The temperature of the PV of the first open-flow flat-plate collector model had decreased by 8.4% as compared to the second model which reduced by 9.8%. Meanwhile, electrical performance of the panels was 23.9% and 25.3% improved in the first and second configuration respectively.
Sopian et al. [44]	Experimental	2011	Parallel-flow and Split flow	The split-flow collector is also more efficient in terms of thermal performance than the parallel collectors and direct, which operate independently, and the influx of cold water on both sides of the face, hence the superior performance of the split-flow collector in an academic environment.

2. Experimental setup

2.1. Innovative design and construction of a PVT system

The analyzed PV-M is a monocrystalline glass-glass model, and the main parameters of the PV-M under the standard test conditions (STC) are outlined in Table 2. In order to enhance the thermal control while conserving the EEF of the cells, we came up with a new stainless-steel heat-exchanger geometry, thus addressing the inadequacies pointed out in the existing literature. In this configuration, each row of PV cells is in direct contact with a thin layer of water 10 mm thick (Fig. 1), promoting more efficient heat transfer and uniform temperature regulation on the surface of the cells. To optimize both structural support and fluid circulation, a hollow channel was designed between each adjacent cell (Fig. 2). This channel allows for continuous laminar flow of water from the inlet to the outlet of the system, while keeping the cells securely attached to their support, thereby reducing temperature gradients and minimizing hot spots. The system also includes two 30 mm high manifolds that distribute the water evenly across the various layers of the exchanger. Each water layer is equipped with specific supply and outlet areas, ensuring a steady flow. When started up, the water first fills the inlet manifold and then gradually circulates through the channels of each layer, ensuring even distribution to the outlet point. The exchanger is attached to the PV-M using a high-conductivity thermal paste, ensuring efficient heat transfer between the cells and the water. The different phases of assembly and experimental manufacturing are shown in Fig. 3.

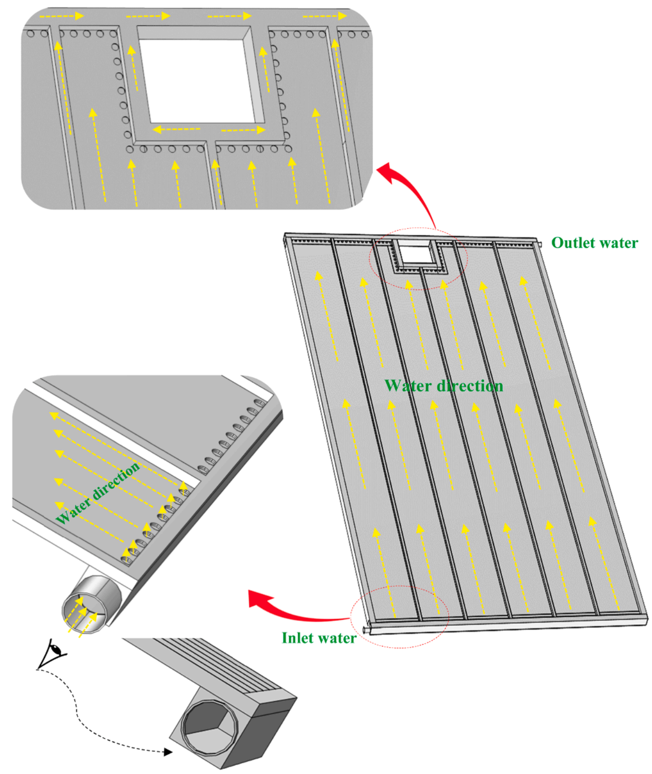

Fig. 1. Complete configuration of the stainless steel heat exchanger with direct water circulation between the PV cells.

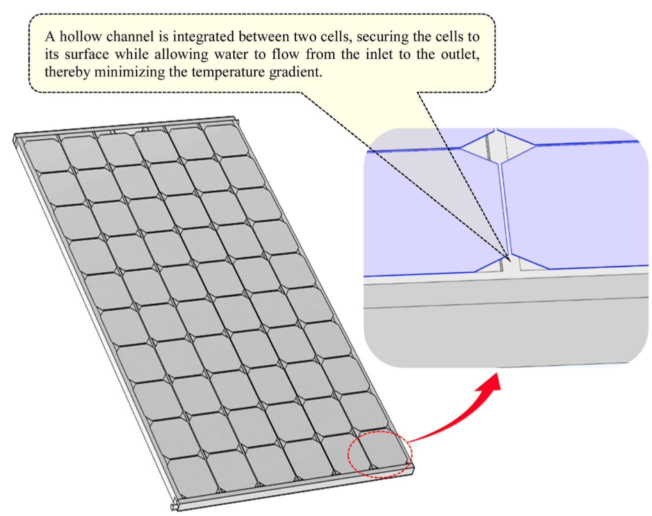

Fig. 2. Integrated hollow channel for uniform water circulation and PV cell attachment.

Table 2
Technical data and performance of the Almaden SEAC60T-300 monocrystalline glass-glass PV-M evaluated under STC.

Parameters	Value	Unit	Symbol
Temperature coefficient of maximum power	−0.39	%/ °C	-
Rated (nominal) power	300	W	P_{max}
Maximum power point voltage	32.40	V	V_{mpp}
Module surface area	1.64538	m^2	A
Short-circuit current	9.73	A	I_{sc}
Temperature coefficient of open-circuit voltage	−0.3	%/°K	-
Open-circuit voltage	39.87	V	V_{oc}
Conversion efficiency	18.237	%	η_{ref}
Maximum power point current	9.26	A	I_{mpp}
Temperature coefficient of short-circuit current	0.06	%/°K	-

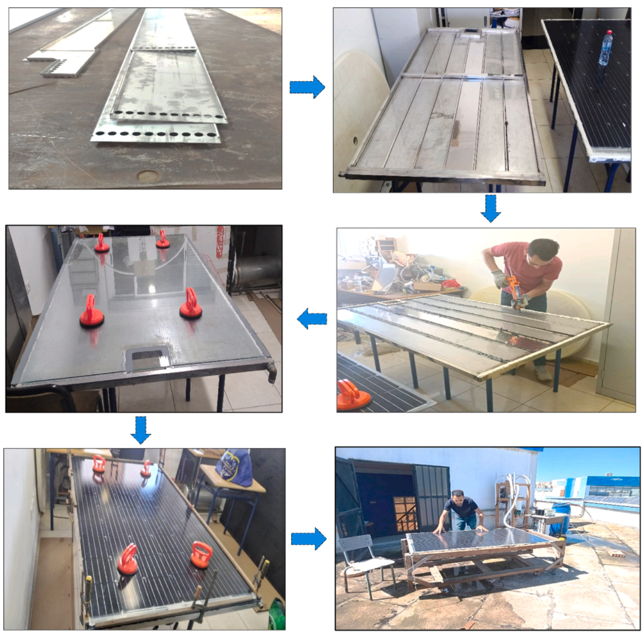

Fig. 3. Steps for assembling and experimentally implementing the new PV design.

2.2. Experimental arrangement and measurement instrumentation

The experimental setup was designed to simultaneously evaluate the electrical and thermal performance of a PV-M used as a reference and a PVT-S installed side by side, ensuring identical experimental and technical conditions for both configurations. The water circulating in the PVT-S exchanger captures the heat generated by the PV cells, raising its temperature and allowing it to be used for practical applications, as illustrated in Fig. 4. An open-loop pump facilitates fluid circulation, ensuring a constant flow throughout the system. A flow meter and manual valve are used to ensure precise control and regulation of water flow and, consequently, the reproducibility of measurements within the experiment. The water required to operate the PVT-S system is also stored in a 30-liter tank filled with drinking water, ensuring a constant and reliable water supply to carry out the experiment.

The complete experimental setup, which includes all sensors and equipment ordered to test the performance of the PVT-S and the reference PV-M, is shown in Fig. 5. This setup allows simultaneous measurement of the electrical and thermal processes of both devices under the same conditions. The water contained in the PVT-S is pumped using an open-circuit pump; the flow rate can be adjusted using a manual valve and monitored using a MAG-VIEW MVM-030-PA flow meter, which ensures a constant and reproducible flow. The temperature of the fluid entering the device is measured using a mercury thermometer, but the outlet temperature is measured to determine the degree of heat recovery. In order to analyze the heat distribution in the modules, four type K thermocouples had to be attached to each panel and connected to an Arduino Mega board, which allowed automated measurements to be taken every ten minutes. An I-V tracer was used to obtain electrical measurements, such as voltage, power, current, and provided accurate information on the power generated by the panels. At the same time, the ambient temperature was recorded using a SOLAR-02 sensor, and solar irradiance was measured using an HT304N reference cell, allowing the module's performance to be correlated with environmental conditions. The thermal distribution of the panel surfaces was mapped using an infrared camera, which provided a detailed description of the heat transfer processes and enabled the detection of overheated areas. The technical specifications of all the devices used are summarized in Table 3, which ensured the traceability of the measurements and reinforced the validity of the results obtained in the experiment.

2.3. Measurement uncertainty

To measure the quality of the obtained measurements, a detailed examination of the sources of errors and experimental uncertainties was carried out. Table 3 shows the tolerances and technical specifications that have been supplied by the manufacturers of each apparatus. With this information combined with a 95% confidence interval [26], we were able to determine the cumulative effect of errors upon the results.

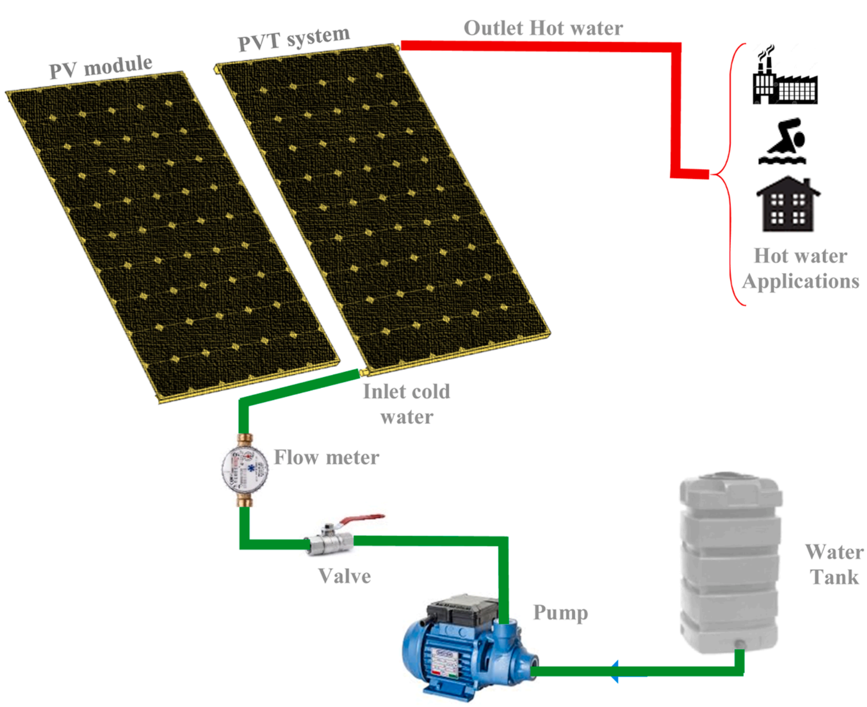

Fig. 4. Functional diagram of the experimental setup and cooling circuit of the PVT-Ss.

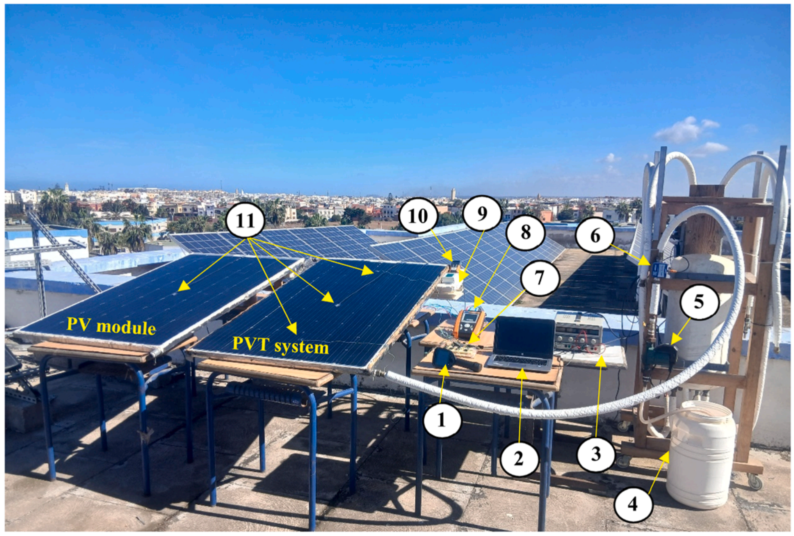

Note: (1) Infrared camera, (2) Computer, (3) Mercury thermometer, (4) Water reservoir, (5) Pump, (6) Flow meter, (7) Data acquisition and transmission system, (8) I-V tracer, (9) HT304n reference cell, (10) SOLAR -02 sensor, and (11) Thermocouples.

Fig. 5. Complete experimental setup with instrumentation for monitoring the PVT-S and PV-M.
Note: (1) Infrared camera, (2) Computer, (3) Mercury thermometer, (4) Water reservoir, (5) Pump, (6) Flow meter, (7) Data acquisition and transmission system, (8) I-V tracer, (9) HT304n reference cell, (10) SOLAR −02 sensor, and (11) Thermocouples.

Table 3
Summary of experimental instruments and their main characteristics.

Equipment and models	Used to measure	Measurement range	Uncertainty
HT304N reference cell	Incident solar irradiance	50–1400 W/m^2	± 3.0%
Mercury thermometer	Fluid inlet temperatures	0 °C to 100 °C	± 0.5 °C
Thermocouple (type K)	Module and fluid outlet temperature	−200 °C to +1350 °C	± 2%
HT I-V400 solar tracer	Electrical quantities (voltage, current, power)	-	1%
FLIR E5 Pro infrared camera	Temperature distribution across modules	−20 °C to 400 °C	± 2%

The total uncertainty generated by the device, calculated according to Eq. (1) [45], was estimated to be ± 4.24, which is less than the critical 5% mark [26], this shows that the experiment results are a true reflection of the actual behavior of both PV and PVT-Ss systems. The rigor of the methodology highlights the strength of our method and strengthens the validity of the conclusions reached on the basis of thermal and electrical analysis of the panels.

$$\psi Y = \sqrt{\left(\frac{\partial Y}{\partial H_1}\psi_1\right)^2 + \left(\frac{\partial Y}{\partial H_2}\psi_2\right)^2 + \ldots\ldots + \left(\frac{\partial Y}{\partial H_n}\psi_n\right)^2} \quad (1)$$

Where ΨY indicates the efficiency uncertainty and is influenced by the dependent variables H_1 to H_n.

2.4. Fundamental theory and evaluation

2.4.1. Energy analysis

The distribution of solar energy captured by the module can be studied by considering the entire PVT-S as a single control volume, shown schematically in Fig. 6. In this approach, the incident energy ($\dot{E}_{in}$) is transformed into three main contributions: a portion transferred to the heat transfer fluid in the form of useful heat ($\dot{E}_{th}$), a fraction converted into electricity ($\dot{E}_{el}$), and finally a quantity dissipated into the environment in the form of heat losses ($\dot{E}_{loss}$). Under steady-state conditions, these different contributions are linked by the energy balance formulated in Eq. (2) [46].

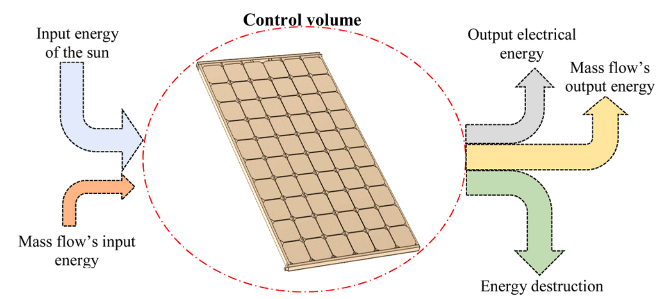

Fig. 6. Control volume model adopted to establish the energy balance of the PVT-S.

$$\dot{E}_{in} = \dot{E}_{loss} + \dot{E}_{th} + \dot{E}_{el} \quad (2)$$

The amount of energy captured by the PV-M depends on the solar flux incident on its active surface A_{PV} and the irradiance level G, as expressed in Eq. (3). The electrical conversion of this energy is then determined based on the characteristics of the module, in particular the open-circuit voltage V_{oc} and the short-circuit current I_{sc}, in accordance with Eq. (4). Finally, the form factor (FF), calculated using Eq. (5), summarizes the electrical behavior of the panel and its ability to produce maximum power from the solar energy received [3,34,47].

$$\dot{E}_{sun} = A_{PV} \bullet G \quad (3)$$

$$\dot{E}_{el} = V_{oc} \bullet I_{sc} \bullet FF \quad (4)$$

$$FF = \frac{P_{max}}{V_{oc} \bullet I_{sc}} = \frac{V_{max} \bullet I_{max}}{V_{oc} \bullet I_{sc}} \quad (5)$$

The quantification of useful thermal energy is performed according to Eq. (6), while Eqs. (7), (8), and (9) are used to evaluate electrical, thermal, and overall efficiency, respectively [48–50]:

$$\dot{E}_{th} = \dot{m}_f \bullet c_{p,f} \bullet (T_{f,out} - T_{f,in}) \quad (6)$$

$$\eta_{el} = \frac{\dot{E}_{el}}{\dot{E}_{sun}} \quad (7)$$

$$\eta_{th} = \frac{\dot{E}_{th}}{\dot{E}_{sun}} \quad (8)$$

$$\eta_{ov} = \frac{\dot{E}_{el} + \dot{E}_{th}}{\dot{E}_{sun}} \quad (9)$$

2.4.2. Exergy analysis

The exergy approach makes it possible to quantify the fraction of solar energy that can actually be exploited by the system, taking into account internal losses and thermodynamic irreversibility. From this perspective, the total exergy of the device, considered as a steady-state control volume (Fig. 7), is expressed by Eq. (10) as the sum of four contributions: the exergy provided by solar radiation ($\dot{X}_{sun}$), the recovered thermal exergy ($\dot{X}_{th}$), the generated electrical exergy ($\dot{X}_{el}$), and the exergy lost due to internal irreversibility ($\dot{X}_{des}$). The incoming solar exergy is determined using Eq. (11), adopting a solar temperature T_{sun} of 5770 K, while Eqs. (12) and (13) are used to calculate the thermal exergy and electrical exergy, respectively [4,51,52].

$$\dot{X}_{sun} = \dot{X}_{des} + \dot{X}_{el} + \dot{X}_{th} \quad (10)$$

$$\dot{X}_{sun} = G \bullet A_{PV} \bullet \left[1 - \frac{4}{3}\left(\frac{T_{amb}}{T_{sun}}\right) + \frac{1}{3}\left(\frac{T_{amb}}{T_{sun}}\right)^4\right] \quad (11)$$

$$\dot{X}_{th} = \dot{m}_f \bullet c_{f,p} \bullet \left(1 - \frac{T_{amb}}{T_{f,out}}\right) \bullet (T_{f,out} - T_{f,in}) \quad (12)$$

$$\dot{X}_{el} = \eta_{el} \bullet G \bullet A_{PV} \bullet \left[1 - \frac{4}{3}\left(\frac{T_{amb}}{T_{sun}}\right) + \frac{1}{3}\left(\frac{T_{amb}}{T_{sun}}\right)^4\right] \quad (13)$$

Electrical exergy, thermal exergy, and overall exergy efficiency are calculated using Eqs. (14), (15), and (16), respectively [4,5]:

$$\varepsilon_{el} = \frac{\dot{X}_{el}}{\dot{X}_{sun}} \quad (14)$$

$$\varepsilon_{th} = \frac{\dot{X}_{th}}{\dot{X}_{sun}} \quad (15)$$

$$\varepsilon_{PVT} = \varepsilon_{el} + \varepsilon_{th} = \frac{\dot{X}_{out}}{\dot{X}_{sun}} = 1 - \frac{\dot{X}_{loss}}{\dot{X}_{sun}} \quad (16)$$

2.4.3. Exergy destruction and entropy generation analysis

Eqs. (17) and (18), relating to exergy losses and entropy generation, respectively, enable the degradation of usable energy in the PVT-S to be assessed. These effects result from internal irreversibility, in particular, friction in the flow channels and suboptimal heat transfer, and directly influence the effective efficiency of the system [52,53]:

$$\dot{X}_{des} = \dot{X}_{sun} - \dot{X}_{el} - \dot{X}_{th} \quad (17)$$

$$\dot{S}_{gen} = \frac{\dot{X}_{des}}{Tamb} \quad (18)$$

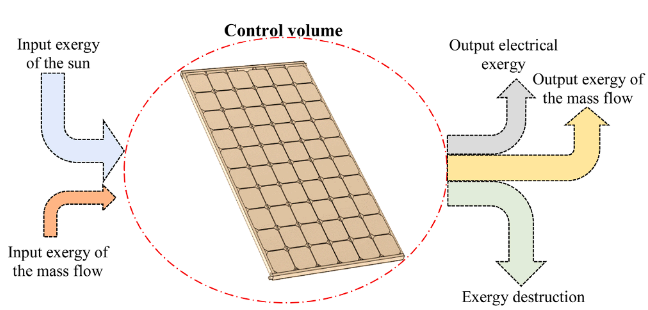

Fig. 7. Control volume model adopted to establish the exergy balance of the PVT-S.

2.4.4. Sustainability metrics analysis

Optimization of resources and the exploitation of renewable sources of energy are critical foundations that must be obligatory in sustainable development. Exergy analysis has been used as a key analytical tool to evaluate a system's performance against an unattainable ideal, isolate thermodynamic losses, and offer the prospect of improving operational efficiency. Due to its inherent association with energy consumption and environmental implications, exergy allows for a rigorous assessment of sustainability using a set of quantitatively defined measures: the sustainability index (SI), which is the derivative of exergy efficiency, as shown in Eq. (19); the wasted exergy ratio (WER), which is the ratio of wasted exergy, as expressed in Eq. (20); and the improvement potential (IP), which is the possibility of reducing losses and mitigating environmental impact, as defined in Eq. (21). Finally, the Ecological Efficiency Index (EcEI) is an integrative index that combines measures of exergy with measures of ecological footprint to provide a holistic assessment of sustainability; specifically, the higher the value of the EcEI, the more sustainable the prudent and environmentally responsible utilization of the available resources (Eq. (22)) [54,55].

$$SI = \frac{1}{1 - \varepsilon_{PVT}} \quad (19)$$

$$WER = \frac{\dot{X}_{des}}{\dot{X}_{in}} \quad (20)$$

$$IP = (1 - \varepsilon_{PVT}) \bullet \dot{X}_{des} \quad (21)$$

$$EcEI = 2 \bullet \varepsilon_{PVT} - 1 \quad (22)$$

2.4.5. Annual energy production analysis

The degradation rate (d_g) of PV-Ms, set at 0.8% per year by the manufacturer, is taken into account along with the annual solar radiation (G_t) measured in El Jadida to calculate the annual energy production of PV and PVT-Ss using Eqs. (23), (24), and (25). The average daily irradiance in the city of El Jadida is 713.7 W/m^2, with an average of 7 h of sunshine per day. These calculations make it possible to evaluate the systems' capacity to generate energy over their entire lifespan and provide a solid basis for analyzing their economic viability [54,56].

$$E_{ele} = (365 \bullet G_t \bullet \eta_{el} \bullet A_{PV}) \bullet (1 - dg)^{t-1} \quad (23)$$

$$E_{th} = (365 \bullet G_t \bullet \eta_{th} \bullet A_{th}) \bullet (1 - dg)^{t-1} \quad (24)$$

$$E_{ntotal} = E_{th} + E_{ele} \quad (25)$$

2.4.6. Enviro-economic (environmental cost) analysis

The emission of CO_2 is the primary focus of the energy transition to be sustainable. In this context, PV and PVT technologies give a worthy benefit since they generate electricity without emissions of greenhouse gases. To be able to assess the environmental effects of these systems, the current research compares an energy-gain analysis with an approximation of the avoided CO_2 emissions. The annual CO_2 reduction $\varnothing_{CO_2}$ (in tCO_2/year) for the new PVT-S and for the reference PV-M is determined using Eq. (26), where ψ_{CO2} corresponds to the specific CO_2 emissions for electricity production from coal (2.08 kg CO_2/kWh), n represents the average number of hours of sunshine per year, and $\dot{Q}_u$ denotes the average energy gain calculated using Eq. (27). The environmental cost (Z_{CO_2}) associated with this reduction is then evaluated using Eq. (28), using an average carbon price (P_{CO_2}) set at 14.5 $ per ton of CO_2 [57,58].

$$\O_{CO_2} = \frac{\dot{Q}_u \times \psi_{CO_2} \times n}{1000} \tag{26}$$

$$\dot{Q}_u = \dot{E}_{th} + \frac{\dot{E}_{el}}{0.38} \tag{27}$$

$$Z_{CO_2} = P_{CO_2} \times \O_{CO_2} \tag{28}$$

2.4.7. Economic and financial viability analysis

In order to calculate the amount of energy initially impacted by systems under consideration, the energy consumed in the production of the systems should be estimated. This method is founded on the principle of embodied energy and involves all the energy that is used in materials, production processes, and assembly tasks. This research aims to estimate the quantity of energy required to build the experimental system, followed by a comparison with the quantity of energy generated in a year as well as the reduction in emissions. The gray energy of PVT and PV systems has been calculated through Eq. (29) [9,59], and used as a reference when calculating the preliminary energy needed to design PVT and PV systems.

$$Embodiedenergy = \frac{CapitalCost}{0.14} \tag{29}$$

Among the major indicators that one can use to measure the energy efficiency of PVT and PV systems is the amount of time it takes the installation to pay back the energy that it used during its production. This parameter is referred to as PBT hence, the number of years taken to recover the energy that was invested. It is determined by Eq. (30), which forms a direct relationship between the embodied energy of the system and its yearly production [9,59].

$$PBT = \frac{Embodiedenergy}{Annualenergyoutput} \tag{30}$$

The economic evaluation of an electricity generation system is often based on the levelized cost of electricity (LCOE), which represents the average cost of producing one unit of electricity over the lifetime of the system. For PV and PVT systems, the LCOE is calculated using Eq. (31). The initial cost of the system, denoted C_0, also includes installation costs, estimated at 1% of this cost. Added to this are annual maintenance expenses A_t, assumed to be 10% of the initial cost. The lifetime n is set at 25 years, and the discount rate i is taken to be 5%. The annual electricity savings, $M_{t,el}$, are determined using Eq. (9) and enable the energy gains achieved each year to be quantified [9].

$$LCOE = \frac{C_0 + \sum_{t=1}^{n} \frac{A_t}{(1+i)^t}}{\sum_{t=1}^{n} \frac{M_{t,el}}{(1+i)^t}} \tag{31}$$

3. Three-dimensional simulation study

COMSOL Multiphysics® software, based on the FEM, was used to perform an in-depth numerical analysis of the new PVT-S. The 3D simulation, carried out in steady state, made it possible to accurately characterize the heat transfer and fluid behavior within the system. The model is based on the actual geometry of the device and takes into account all components of the monocrystalline silicon PV-M. The stainless-steel heat exchanger and expanded polystyrene insulation were integrated into the model, with the effect of the latter being considered indirectly via boundary conditions. The PV cells, surrounded by the upper and lower EVA layers, are placed between the upper and lower glass, allowing the electrical and thermal behavior of the module to be accurately reproduced. Table 4 provides details on the size and thermal properties of each component, while Table 5 presents information on the optical characteristics and environmental conditions considered in the modeling.

Table 4
Dimensional and thermal characteristics of PVT-S components [5,60,61].

Material Layer	Thickness (mm)	ρ (kg/m³)	C_p (J/kg.K)	k (W/m.K)
Water	-	998	4181.8	0.68
Stainless steel	-	8030	502.48	16.27
Silicon	0.19	2329	703	148
Glass	2.5	2200	750	1.8
EVA	0.5	935	2400	0.29

Table 5
Environmental parameters and optical characteristics considered in the modeling [4,62].

Description	Values	Symbol / Unit
PV-M packing factor	0.95	P_c
Optical transmittance of the glass	0.96	τ_g
Convective heat transfer coefficient at glass-air interface	10	$U_{g\text{-}amb}$ (W/m².K)
Emissivity of the glass layer	0.04	ε_g
Absorption coefficient of the PV cell	0.9	α_c
Reference operating temperature	25	T_{ref} (°°C)

3.1. Governing equations

The heat generated by the PV cells is transferred to the solids in the PVT-S exclusively by conduction, allowing it to be transferred to the heat transfer fluid, as shown in Eq. (32). Once in the channel, the fluid exchanges heat through a mechanism combining conduction and convection, represented by Eq. (33) for water. The behavior of the fluid is then described through the equations of conservation of mass (Eq. (34)) and momentum (Eq. (35)), ensuring a complete modeling of heat transfers and hydrodynamic flow within the system [63,64].

$$\nabla \bullet (k \nabla T) = 0 \tag{32}$$

$$\rho C_p \frac{\partial T}{\partial t} + \rho C_p u \bullet \nabla T = \nabla \bullet (k \nabla T) + Q \tag{33}$$

$$\rho \frac{\partial u}{\partial t} + \nabla \bullet (\rho u) = 0 \tag{34}$$

$$\rho \bullet \frac{\partial u}{\partial t} + \rho (u \bullet \nabla) u = \nabla \bullet \left[-pI + \mu \left(\nabla u + (\nabla u)^T \right] + F \tag{35}$$

3.2. Boundary conditions

The boundary conditions employed in the simulation are summarized in Fig. 8. For the upper surface of the module, several thermal phenomena are taken into account in order to accurately represent interactions with the environment. First, this surface receives external energy input, modeled by Eq. (36), where the temperature of the glass (T_g) and its thermal conductivity (kg) are used in the expression of the

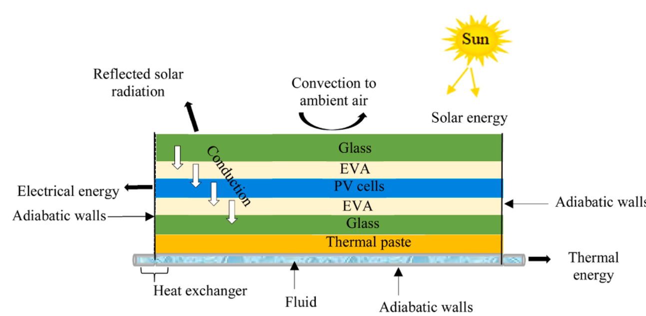

Fig. 8. Distribution of boundary conditions on the different surfaces of the PVT-S.

applied flux. Next, this same surface exchanges heat with the ambient air by convection, in accordance with Eq. (37). This relationship uses the ambient temperature (T_{amb}), the glass-air convection coefficient (h_{g_amb}), and the direction normal to the wall. Finally, radiative exchanges with the sky are taken into account through Eq. (38). In this expression, T_{sky} represents the effective radiative temperature of the sky, used to estimate radiation losses.

$$-k_g\frac{\partial T_g}{\partial z} = G \tag{36}$$

$$-n \bullet q = h_{g-amb} \bullet \left(T_{amb} - T_g\right) \tag{37}$$

$$-n \bullet q = \varepsilon_g \bullet \sigma \bullet \left(T_{sky}^4 - T_g^4\right) \tag{38}$$

In the numerical model, the fluid-solid interface is treated as a thermal coupling zone, which allows the heat exchange between the absorbing conduit and the circulating water to be represented correctly. The insulating materials integrated into the structure are also taken into account in order to limit heat loss to the outside. Regarding the conditions applied to the fluid, Eq. (39) sets the input parameters for the channel, namely the fluid temperature and the imposed flow rate. The behavior of the flow in contact with the walls is governed by Eq. (40), which imposes a no-slip condition. At the outlet of the domain, Eq. (41) defines a relative pressure equal to zero, and no viscous stress is applied, ensuring free flow at the end of the channel.

$$T = T_{in}, \dot{m} = \dot{m}_{in} \tag{39}$$

$$u = 0, v = 0, w = 0 \tag{40}$$

$$P_{out} = 0 \tag{41}$$

3.3. Principal assumptions governing the model

For the numerical solution of the PVT-S using the Conjugate Heat Transfer module in COMSOL Multiphysics®, several simplifying assumptions were introduced to make the model more manageable and physically consistent:

✓ Ethylene vinyl acetate (EVA) is considered completely transparent to solar radiation [65].
✓ The heat transfer fluid is modeled in steady state, with laminar and incompressible behavior [63].
✓ The side walls and base of the module are considered to be perfectly insulated, eliminating any heat loss to the outside [3,4].
✓ The influence of dust on the transmission and absorption of solar radiation is neglected, as the module surface is assumed to be clean [62,66].
✓ The thermophysical properties of materials are assumed to be constant despite temperature variations [67].

3.4. Mesh refinement and independence study

A mesh convergence study was conducted before the main simulations to make sure that the numerical results of the PVT-S were accurate and strong. The mesh combined tetrahedral elements for the main volume and triangular elements on the surfaces, accompanied by boundary layer refinement to better represent the strong thermal gradients near the walls and PV cells (Fig. 9). For this test, the operating conditions were set at a water flow rate of 0.05 kg/s and an irradiance of 1000 W/m^2. The maximum fluid pressure was monitored across five mesh density levels, ranging from 514,750 to 3804,079 elements. The analysis showed that increasing the number of elements beyond 1675,550 produced negligible variations in maximum pressure (Fig. 10), indicating that the model was mesh-independent. On this basis, a mesh of 1675,550 elements was chosen for all subsequent simulations, achieving an optimal compromise between accuracy and computation time. This configuration ensures that the relative error on the maximum pressure remains below 1%, thus ensuring the reliability of the numerical results.

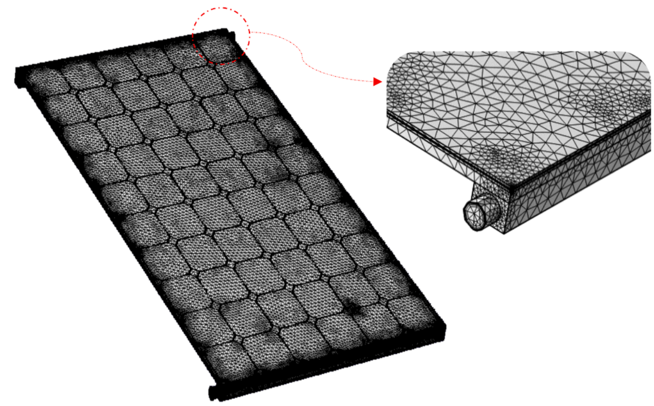

Fig. 9. Mesh used for the PVT-S, including tetrahedral and triangular elements and boundary layers.

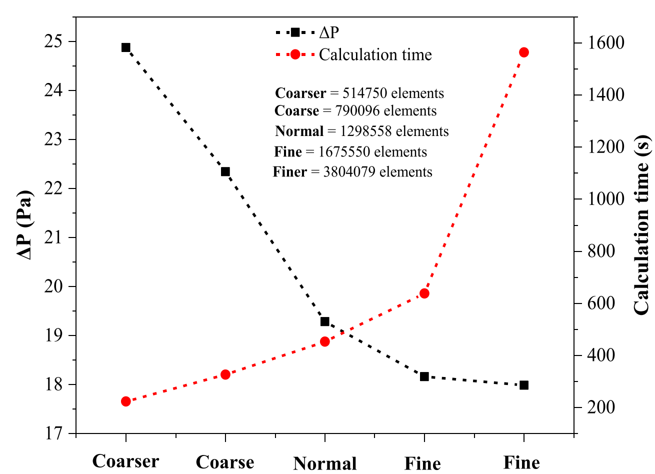

Fig. 10. Grid independence study based on maximum fluid pressure.

4. Results and discussion

4.1. Environmental conditions

The new PVT-S was tested experimentally in El Jadida, a Moroccan coastal city on the Atlantic coast (Fig. 11a) [68], located 96 km southwest of Casablanca at an average altitude of 10 m. This location has high ambient humidity, particularly in the early morning and evening, which means that measurements must be limited to periods when humidity is at its lowest in order to protect sensitive instruments such as the I-V tracer. The experiments were therefore conducted between 11h44 and 18 h (Fig. 11b) on September 12, 2025, with a water flow rate of 0.0556 kg/s. The mass flow rate of the heat transfer fluid was determined following preliminary tests aimed at ensuring effective cooling of the PV module while limiting hydraulic losses. The flow rate selected represents a compromise between improved thermal performance and stable system operation. During this day, solar radiation rose gradually during the morning, reaching a maximum of approximately 898 W/m^2 between 12 h and 14 h, before decreasing in the afternoon (Fig. 12). The ambient temperature followed a similar pattern, gradually increasing to a peak of 35.5 °C between 14 h and 16 h, then decreasing thereafter. These conditions made it possible to evaluate the thermal and electrical behavior of the PVT-S under conditions representative of a sunny day, while

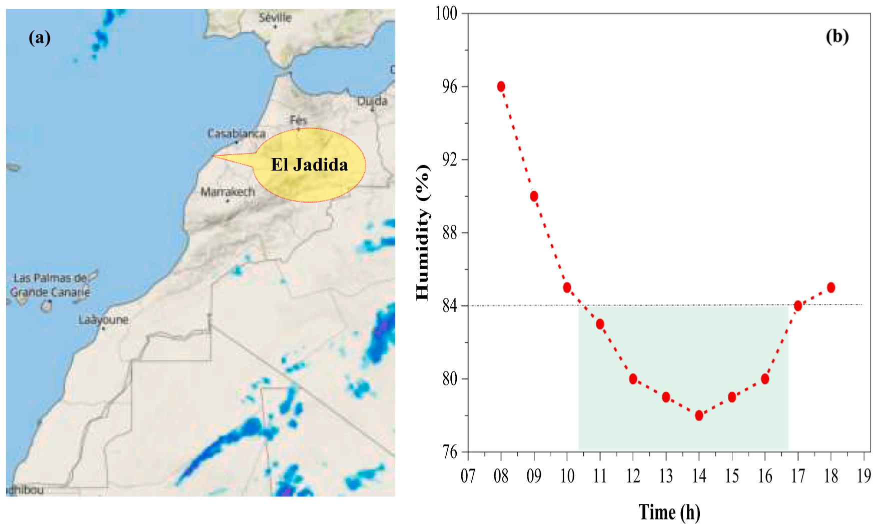

Fig. 11. (a) Location of the city of El Jadida and (b) variation in relative humidity during the measurement day.

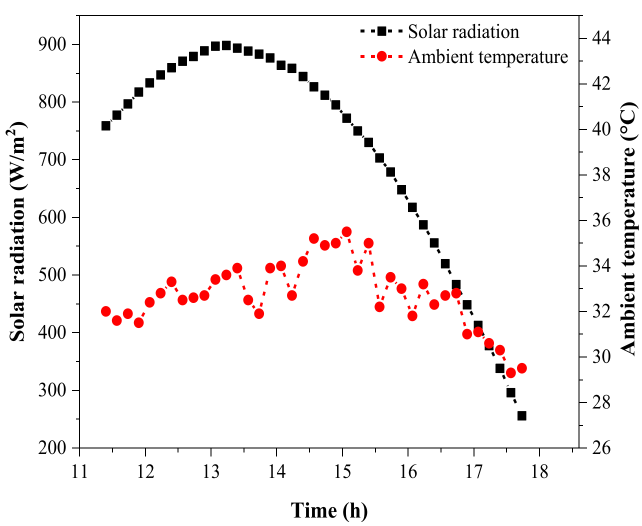

Fig. 12. Variation in solar radiation and ambient temperature recorded on September 12, 2025, during experimental testing of the PVT-S.

ensuring the safety of moisture-sensitive equipment.

4.2. Energy analysis

The temperature profile in the PVT-S under different solar irradiance conditions on the PV cells is shown in Fig. 13. The thermal distribution with increased irradiance indicates that the module is generally heated, with the hottest point being approximately 23.99 °C for irradiance between 200 and 1000 W/m^2. This increase in temperature demonstrates the sensitivity of the semiconductor material to the concentration of incident solar radiation. The cells are much cooler in the heat transfer fluid inlet section. This effect results from immediate contact with a fluid that is still cold, which generates a marked thermal gradient between the upstream and downstream sides of the collector. As the fluid progresses through the pipes, it gradually heats up by capturing the heat extracted from the cells. This increase in temperature slowly reduces its cooling capacity, which explains why the cells at the outlet of the system have a slightly higher temperature. An interesting aspect is observed at the junction box, which is thermally insulated from the fluid. Heat cannot escape in this area, which is therefore marked as the area with the highest temperature, as indicated on the panel. A comparison of the experimental observations shown in Fig. 14 reveals a strong correlation between the simulation and reality. The thermal gradients and the position of the hot spots are also similar, proving the ability of the numerical model to accurately reproduce the thermal behavior of the PVT-S.

Fig. 15 shows how the temperature of the PVT-S changed over time compared to that of the reference PV-M throughout the day. It can be seen that the reference panel reached its maximum temperature of 54.04 °C, while the PVT-S reached a maximum temperature of 34.63 °C, demonstrating the effectiveness of the cooling provided by the heat transfer fluid. This temperature gradient increases with increased solar radiation, leading to a gradual increase in the temperature of the PVT-S. The maximum difference between the two configurations was 19.81 °C. These results confirm that the PVT-S effectively controls cell heating, which is a major advantage in maintaining high EEF and extending the durability of PV-Ms.

During the experiment, the current-voltage (I-V) and voltage-power (P-V) characteristics of the PVT-S and the reference PV-M were measured in order to compare their electrical properties. Analysis of the curves reveals that the PVT-S has a clear advantage over traditional PV-Ms in terms of power and efficiency, as shown in Fig. 16, which compares the evolution of electrical power and efficiency throughout the day. It can be seen that the PVT-S is capable of maintaining better performance, which has been attributed to the positive influence of its integrated thermal management system. Specifically, the PVT has a maximum power of 240.070 W and an efficiency of 16.798, which is lower than the 227.057 W and 15.981% of the PV-M. The results obtained indicate a measurable increase in energy, and the most significant differences, namely 19,110 W of power and 1.255% efficiency, demonstrate the effectiveness of cooling and heat flow optimization.

Fig. 17a shows that the electrical power of both systems increases at noon, in line with the maximum irradiance. This phenomenon can be explained by the increase in incident photon flux, which promotes the formation of electron-hole pairs in the PV cells, leading to a corresponding increase in current, as shown in Fig. 17b This direct relationship between irradiance and current explains why electrical power increases simultaneously. For example, for the PVT-S, an irradiance of 898 W/m^2 corresponds to a power of 240.070 W for a current of 7.704 A, while at 519.5 W/m^2 and 255.85 W/m^2, the power decreases to 139.598 W and 69.218 W, respectively, with currents of 4.310 A and 2.125 A. In contrast, the EEF follows an inverse trend and reaches a minimum at noon, with 16.213% for the PVT-S and 14.992% for the reference PV-M. This decrease can be explained by the increase in cell temperature, which is a direct consequence of high radiation. The increase in

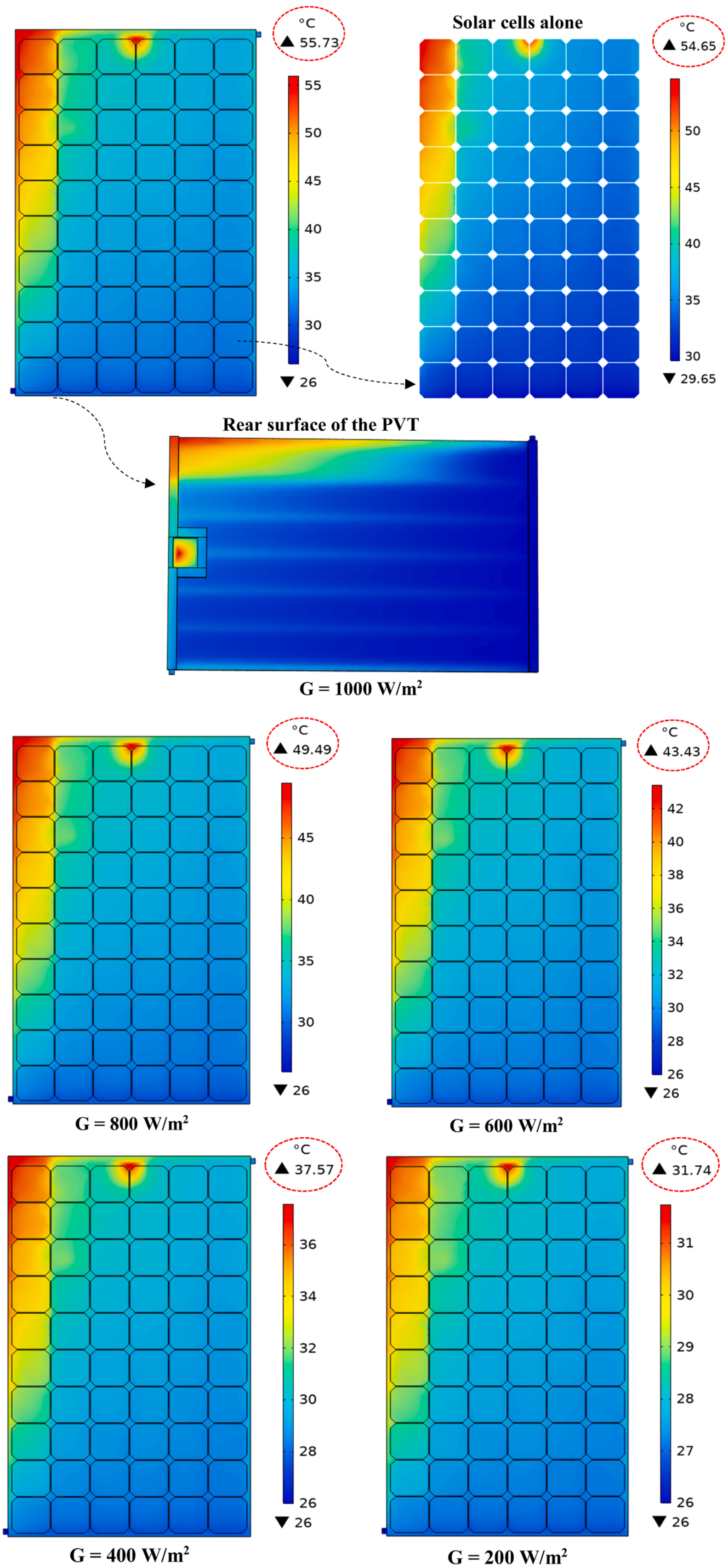

Fig. 13. Thermal distribution of the PV cells of the PVT-S under different levels of solar irradiance, obtained by numerical simulation using COMSOL.

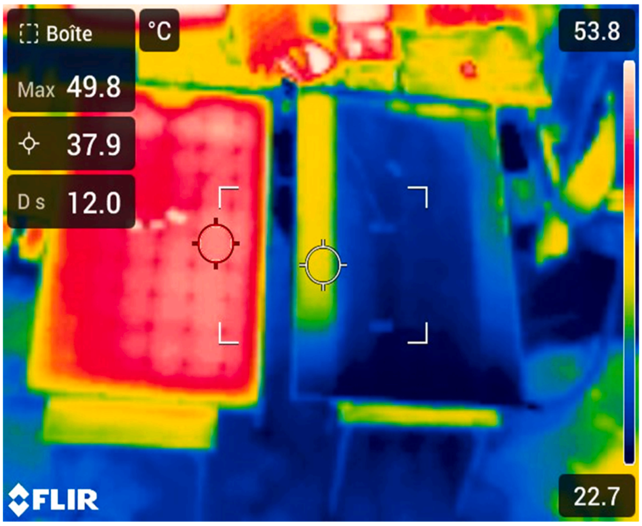

Fig. 14. Experimental thermal image confirming the thermal distribution obtained by numerical simulation in COMSOL.

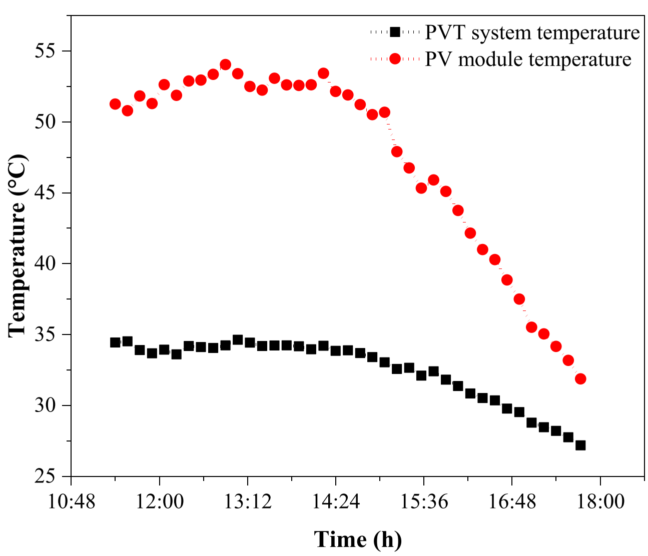

Fig. 15. Comparison of the temperature of the PVT-S and the reference PV-M during the day.

temperature leads to increased recombination of charge carriers and reduces the effective band gap, which decreases the open-circuit voltage. Thus, even if the current increases, the decrease in voltage becomes dominant, as shown in Fig. 18, resulting in an overall reduction in efficiency.

Fig. 19 illustrates the thermal behavior of the PVT-S throughout the day, showing the evolution of the fluid inlet and outlet temperatures as well as the TEF. The inlet temperature remains virtually stable, between 23.75 °C and 25 °C, indicating that the circuit supply remained constant during the measurements. However, the fluid outlet temperature varies according to solar irradiance, reaching a maximum of 29.75 °C at noon before gradually decreasing to 24.75 °C around 5:44 pm. This fluctuation in outlet temperature directly influences TEF, since the latter depends on the fluid's ability to extract heat from the system. The efficiency reached a maximum of 76.885% at 14 h 34, then decreased to a minimum of 37.251% around 17 h 44, with a daily average value of 66.317%.

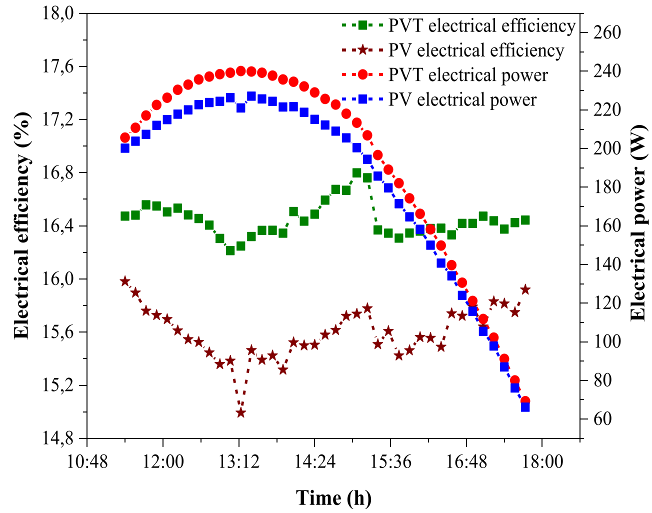

Fig. 16. Comparison of the power and EEF of the PVT-S and the reference PV-M throughout the day.

4.3. Total exergy efficiency, exergy destruction, and entropy generation analysis

In this study, the examination of exergy performance aims to assess the quality of the energy converted by the two systems. Exergy makes it possible to evaluate the useful portion of the available energy, taking into account the irreversibility generated during the process. This section, therefore, analyzes the total exergy of the PVT-S and the PV-M in order to assess their operational behavior throughout the day. Fig. 20 illustrates the evolution of the total exergy efficiency of the two configurations. The average values obtained show that the PV-M achieves an exergy efficiency of 15.597%, while the PVT-S has a slightly lower value of around 15.313%. Contrary to the trends generally reported in the literature, where the PVT-S displays higher exergy efficiency thanks to the simultaneous recovery of electrical and thermal energy, the result observed here is reversed. This peculiarity can be explained by the low exergy available in the fluid, due to low-temperature heat recovery and the significant difference between the ambient temperature and the fluid outlet temperature, as illustrated in Eq. (12), which results in negative thermal exergy. In addition, the thermal irreversibilities associated with heat transfer between the PV-m and the heat transfer fluid further reduce exergy efficiency.

Irreversibility analysis is important in explaining energy losses in PV and PVT-Ss. On this note, the analysis of exergy loss and overall entropy generation of the two configurations is compared in this section, also, using Eqs. (17) and (18). Fig. 21 represents the changes of these parameters in heat transfer daily. The findings indicate that the PV-M and the PVT-S are characterized by high exergy losses, which is in line with their low total exergy efficiency. The thermal exergy in the particular case of the PVT-S is very low resulting in exergy loss similar to that of the PV-M even with heat recovery. Moreover, the overall entropy generation of the PVT-S will be caused by the heat transfer and the friction influence of the fluid that circulated in the system [69]. As observed in the figure, the gradual rise in temperature of surface of the cells, especially at solar noon, increases the heat exchange with the environment, and it increases the entropy generation significantly.

4.4. Analysis of sustainability factors

This section discusses the development of sustainability indicators for the two configurations studied, namely PVT-S and PV-M, over the course of the day. Fig. 22 shows how the sustainability index (SI) varies and the improvement potential (IP) of the two systems. The results

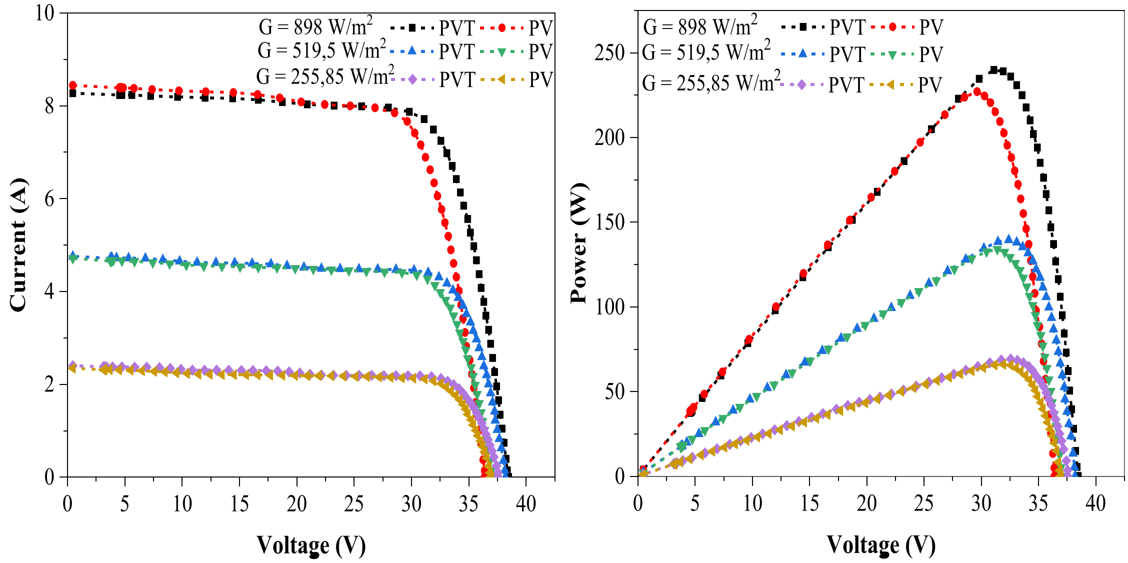

Fig. 17. (a) Current-voltage (I-V) and (b) voltage-power (P-V) characteristics of the PVT-S and PV-M for different solar irradiance values.

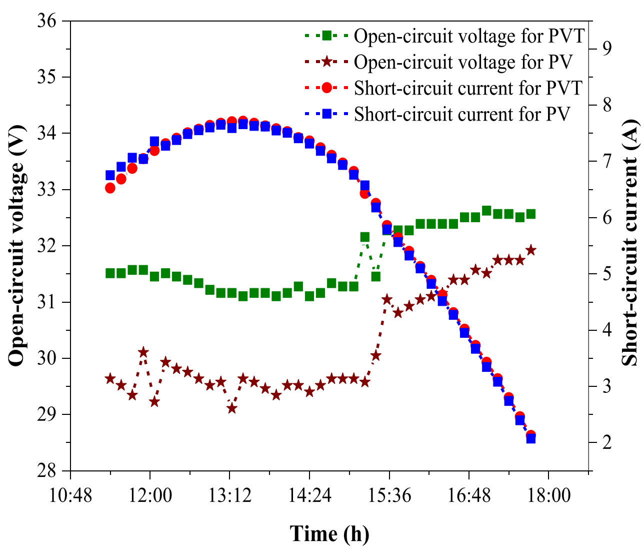

Fig. 18. Evolution of current and voltage in the PVT-S and PV-M over the course of the day.

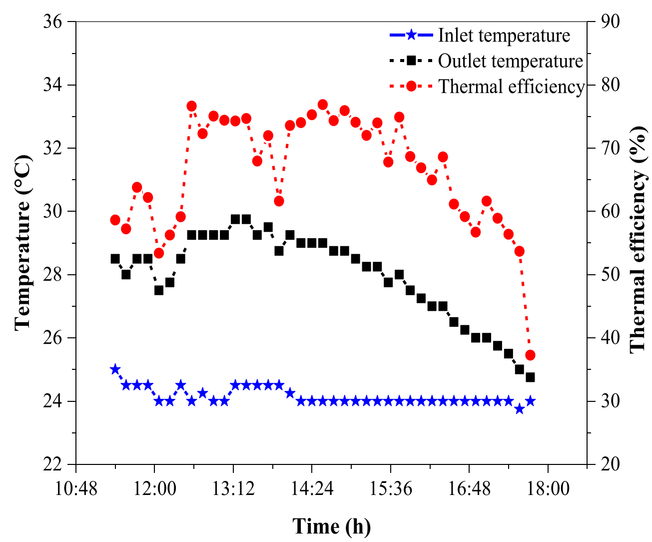

Fig. 19. Daily behavior of fluid temperatures and TEF of the PVT-S.

indicate that the SI tends to increase at the beginning and end of the day and decreases at solar noon. This reduction could be attributed to the substantial increase in cell temperature at that time, due to the increase in irradiance. The maximum values obtained are 1.18883 for the PVT-S and 1.1902 for the PV-M, with respective average values of 1.18084 and 1.1848. The slight superiority of the PV-M is consistent with its higher total exergy efficiency, in accordance with Eq. (16). This figure also shows the evolution of the improvement potential (IP). This increases proportionally to solar irradiance and reaches average values of 783.106 W for the PVT-S and 777.361 W for the PV-M, reflecting the ability of each configuration to efficiently harness the available energy.

The time evolution of the waste exergy ratio and the ecological exergy indicator (EcEI) for PVT-S and PV-M is shown in Fig. 23. The increase in WER with solar irradiance reflects a growing proportion of exergy dissipated as non-recoverable heat, which reflects an intensification of the thermodynamic irreversibilities of the system. For the PVT-S, the WER varies between 0.84117 and 0.90042, indicating greater exergy losses at high irradiance, while for the PV-M, the WER varies between 0.84019 and 0.85007, reflecting overall lower irreversibilities than those of the PVT-S. Conversely, the EcEI decreases as irradiance increases, signaling a deterioration in ecological exergy performance. The EcEI qualitatively assesses the efficiency with which the system uses available energy resources while limiting exergy losses. For the PVT-S, the EcEI ranges from −0.68233 to −0.70831, while for the PV-M, it ranges from −0.68037 to −0.70014. The more negative values observed for the PVT-S indicate a slightly lower exergy ecological performance, mainly due to low-temperature heat recovery and associated thermal irreversibilities.

Furthermore, variations in the heat transfer fluid flow rate can influence these indicators: an increase in flow rate promotes heat extraction and reduces the module temperature, which tends to limit irreversibilities, reduce the WER, and improve the EcEI. On the other hand, a higher ambient temperature reduces the exergy potential of the recovered heat, which increases exergy losses, resulting in an increase in WER and a deterioration in EcEI. Table 6 compares the values of the four indicators for the PVT-S studied with those reported in the literature.

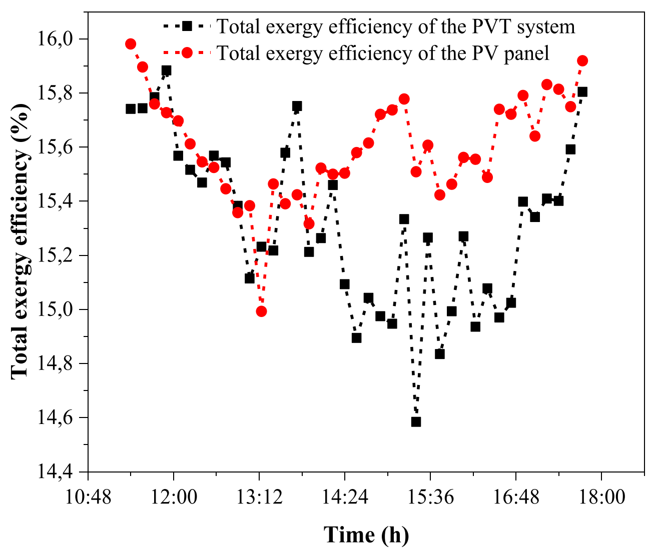

Fig. 20. Evolution of the total exergy yield of the PVT-S and the PV-M during the day.

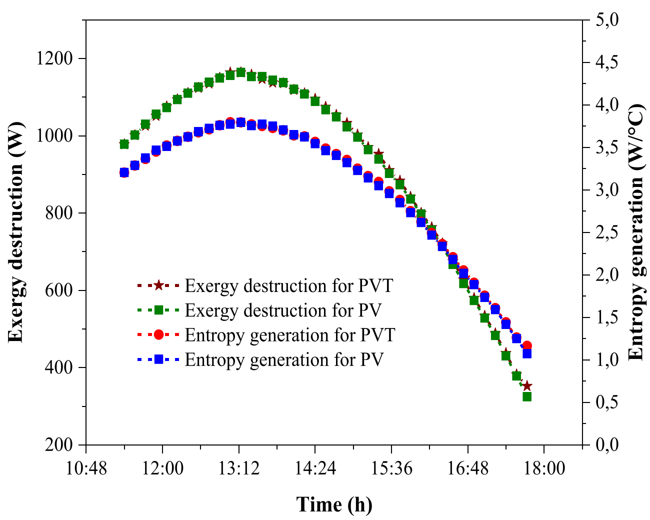

Fig. 21. Daily evolution of exergy loss and entropy generation in the PV-M and PVT-S.

4.5. Annual energy production

Another key aspect in assessing the economic feasibility of a new design is a comparative analysis of the annual energy production between the system under study and a reference PV-M. Fig. 24(a) and (b) illustrate the annual energy production of the PV-M and the PVT-S for the first year. The PV-M produces 534.81 kWh of electricity, without thermal production, while the PVT-S generates 563.86 kWh of electricity and 2274.00 kWh of thermal energy. These results highlight the significant contribution of the PVT-S in terms of thermal energy, leading to a notable improvement in total energy production compared to the PV-M alone and confirming the reliability of the new PVT-S compared to the results of Azeez et al. [56], Rajput et al. [75], and Abo-Zahhad et al. [76]. Fig. 24(c) and (d) show the annual energy production for the 20 years of operation. The electrical production of the PV-M decreases to 459.12 kWh, while the PVT-S reaches a total of 2436.21 kWh. These results show that the energy production of both systems decreases slightly over time due to the aging of materials and the degradation of PV cell performance.

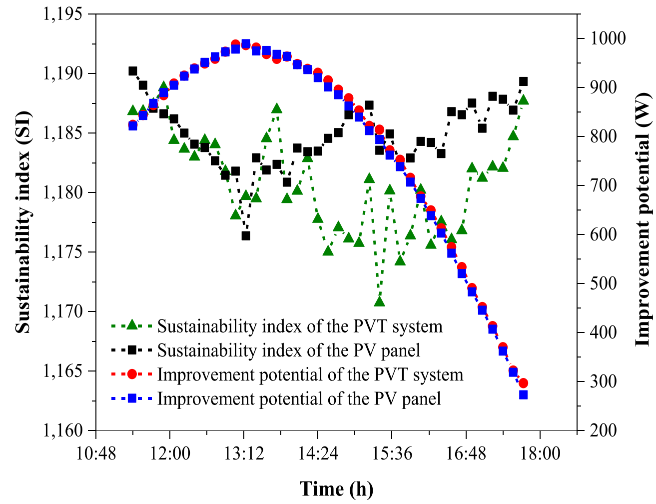

Fig. 22. Daily evolution of the sustainability index (SI) and improvement potential (IP) of the PVT-S and PV-M.

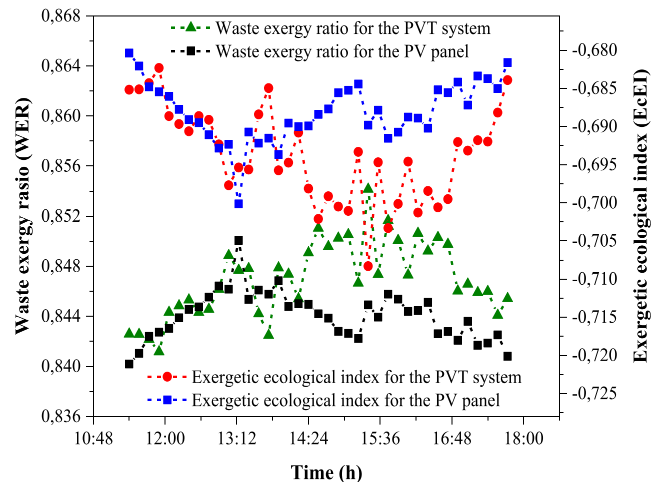

Fig. 23. Daily evolution of the Waste Exergy Ratio (WER) and the Ecological Exergy Indicator (EcEI) for the PVT-S and the PV-M.

4.6. Environmental analysis

The use of renewable energy will play a decisive role in reducing CO_2 emissions from conventional power plants. This study compares the environmental performance of the new PVT-S with that of a reference PV-M in terms of annual CO_2 emissions reduction and environmental cost. The results indicate a reduction in CO_2 emissions of 7922 tCO_2/year for the PVT-S compared to 2920 tCO_2/year for the PV-M, representing a significant difference in environmental performance. Similarly, the annual environmental cost of the PVT-S, estimated at 114,870 $/year, is significantly higher than that of PV (42,340 $/year), reflecting the greater impact of the PVT-S on reducing total environmental impacts. This superiority of PVT-S is also highlighted in Table 7, which presents a detailed comparison with other systems published in the literature. These results confirm that the new PVT-S is a more efficient and sustainable solution for minimizing CO_2 emissions and reducing the environmental costs associated with energy production.

4.7. Economic and financial viability

The economic viability of the systems studied can be evaluated with the help of the analysis of the period of the minimum time of the

Table 6
Comparison of the four PVT-S sustainability indicators for a mass flow rate of 0.0183 kg/s with the results published in the literature.

References &year	PVT-S type	IP	SI	EcEI	WER
[70], 2024	PV–heat pump drying system	0.145	2.327	NA	0.83
[71], 2024	PVT-S with water	68–75.5	1.04–1.08	−0.92-(−0.86)	0.935–0.968
[72], 2022	PVT-S with air cooling	351.92–368.84	1.147–1.174	NA	NA
[73], 2024	Rectangular-channel PVT-S	215,647–421,145	1.172–1.186	−0707-(−0687)	0.843–0.854
[74], 2023	Air-type Model-∇ PVT-S	119.09–329.24	1.141–1.157	NA	NA
Present study	Direct-contact water PVT-S	296,825–987,810	1170–1188	−0,7083 – (−0,6823)	0841–0900

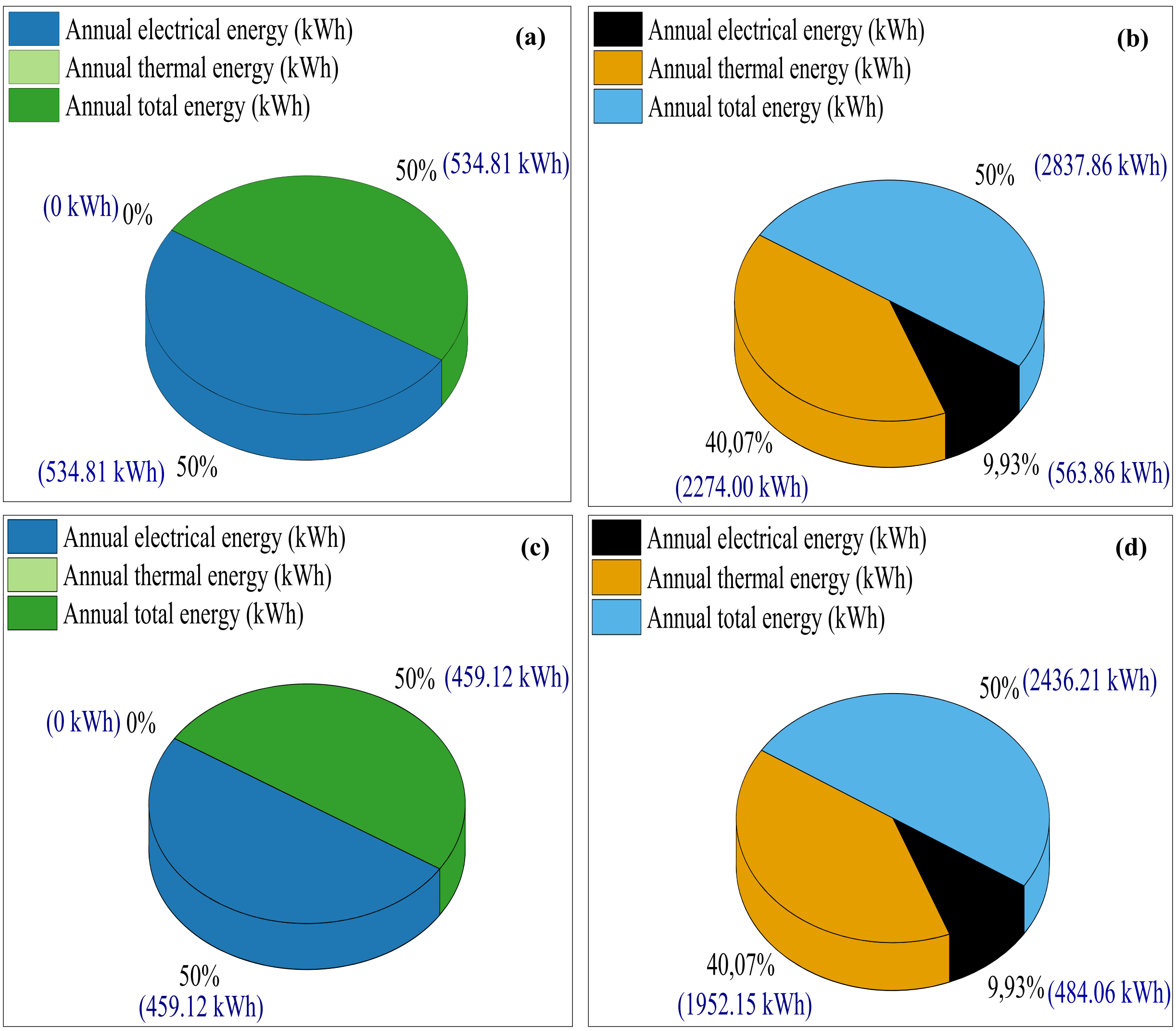

Fig. 24. Annual energy production: (a) PV-M - Year 1; (b) PVT-S - Year 1; (c) PV-M - Year 20; (d) PVT-S - Year 20.

Table 7
Comparison of annual CO_2 emissions reduction and environmental cost for the new PVT-S, PV-M, and systems in the literature.

Reference	System type	$\varnothing_{CO2}$ (tCO_2/ year)	Z_{CO2} ($/year)
Rajput et al. [75]	PV	0.71	10.29
El Alami et al. [57]	PVT	3.610	52.340
Rajoria et al. [77]	PVT	2.523	36.593
Abo-Zahhad et al. [76]	PVT	6.42	93.09
Büyükalaca et al. [78]	PVT	0.815	11.825
Present study	PVT	7922	114,870
	PV	2920	42,340

payback. The overall investments of the new PVT-S are 1870.97 $

Table 8
Total investment cost of new PVT-S and PV-M.

Materials	PVT-S ($)	PV ($)
Heat exchanger	544	-
Thermal paste	64,97	-
Insulation	2.00	-
PV module	200.00	200.00
Water storage tank (200 L)	150	-
Inverter	400	400
Solar controller	60	60
Battery	200	200
Pump	100	-
Water Flow meter	150	-
Total cost ($)	1870.97	860

(Table 8), which is much more expensive than the reference PV-M with costs equal to 860 $ because of the inclusion of more components in the new purchase, like batteries, heat exchangers, insulation, regulators, flow meters, and so forth. This difference is an indication of the influence of the technical complexity and material demands of PVT hybrid systems. Despite this higher initial investment, the payback period for the PVT-S is 4.709 years (Table 9), significantly shorter than that of the reference PV-M, which is 11.486 years. This indicates that the PVT-S allows the initial investment to be recouped more quickly thanks to its ability to produce electricity and thermal energy simultaneously, thereby enhancing its economic profitability over its operational lifetime. The LCOE, representing the average cost of producing one unit of electricity over the lifetime of the system, for the PVT-S is 0.11271 $/kWh (Table 9), slightly higher than the values reported in the literature by Attia et al. [79], who found 0.091 $/kWh, and Kazemien et al. [9], who obtained 0.034 $/kWh. This comparison shows that, although the initial cost of the PVT-S is higher, its ability to generate both electrical and thermal energy gives it better overall economic efficiency. These results highlight the technical and economic advantages of PVT hybrid systems over conventional PV-Ms, particularly for applications requiring optimal energy production and accelerated return on investment.

4.8. Comparative analysis with previously studied PVT systems

Table 10 presents the overall electrical, thermal, and exergy efficiencies of the new PVT-S and compares them to those reported in the literature. Previous research results have shown that the TEF range of PVT-S systems is between 26.87% and 71.29%. This is because these differences cannot be attributed to cooling processes, but depend on a number of variables, including irradiation level, climatic conditions, flow rate, and geographical location. The new PVT-S studied in this study has a TEF of 76.88%, an EEF of 16.79%, and a total exergy efficiency of 15.88%. These results demonstrate that the proposed system offers performance well above that reported in the literature, confirming the effectiveness of the design and optimization of thermal control.

5. Conclusions

This article presents a new PVT-S design that includes a heat exchanger allowing the heat transfer fluid to circulate directly in contact with the rear surface of the PV-M, eliminating the use of the traditional absorber plate. Three-dimensional computational fluid dynamics in COMSOL Multiphysics was used to simulate the system before it was experimentally validated under the weather conditions in El Jadida. Its performance was compared to a comprehensive set of criteria, including energy and exergy efficiencies, thermal distribution, sustainability metrics (improvement potential, residual exergy ratio, ecological efficiency, overall sustainability index, and irreversibility), and environmental and economic indicators (PBT and LCOE). The main findings of this study may be expressed as follows:

- The new PVT-S achieves a maximum temperature difference of 19.81 °C compared to the reference PV-M, with maximum differences of 19.110 W for power and 1.255% for EEF. It achieves a maximum TEF of 76.885%, confirming the effectiveness of cooling and optimization of heat transfer.

Table 9
Return on investment time and LCOE for PVT and PV systems.

System	Embodied energy (kWh)	Annual energy output (kWh/year)	EPBT (Year)	LCOE ($/kWh)
PV	6142.857	534.81	11.486	0,2749
PVT	13,364.071	2837.86	4.709	0,11,271

Table 10
Comparative analysis of the effectiveness of the new PVT-S with previous studies.

References &year	Study type	Fluid type	η_{el} (%)	η_{th} (%)	ε_{PVT} (%)
[46], 2025	Numerical	Serpentine tube	13.9	42	14.2
[80], 2024	Experimental	sheet-and-tube absorber	12.80	43.16	14.0
[81], 2019	Experimental	Serpentine tube	17.33	26.87	14
[82], 2024	Experimental	sheet-and-tube absorber	17.98	57.45	20.68
[83], 2024	Numerical	Serpentine tube	11.15	67.0	12.11–13.93
[84], 2021	Numerical	Rectangular channel heat exchanger	14.17	71.29	14.12
[85], 2024	Numerical	Serpentine tube	11.806	63.159	15.38
[86], 2018	Experimental	Sheet-and-parallel-tube heat exchanger	13.80	37.51	12.68
[87], 2025	Numerical	Perforated twisted tape	12.824	40.63	15.77
Present study	Experimental	Direct-contact water PVT-S	16.79	76.88	15.88

- The new PVT-S achieves an average total exergy efficiency of 15.313%, with exergy destruction of 924.712 W and entropy generation of 3.020 W/ °C, indicating effective management of thermodynamic losses and confirming the overall improvement in system performance and efficiency.
- The PVT-S has an average sustainability index of 1.18084, an average improvement potential of 783.106 W, an average Waste Exergy Ratio of 0.84837, and an average ecological exergy indicator of −0.69373, reflecting good energy performance while highlighting the losses and environmental impact associated with the system's operation.
- The new PVT-S shows a total annual energy output of 2837.86 kWh, well above the 534.81 kWh of the reference PV-M. It reduces CO_2 emissions by 7.922 tCO_2/year compared to 2.920 tCO_2/year for PV, and has an annual environmental cost of 114,870 $/year, highlighting a significant improvement in environmental performance compared to conventional PV-Ms.
- The new PVT-S, with an investment cost of 1870.97 $, has a payback period of 4.709 years and a LCOE of 0.11271 $/kWh, compared to 860 $ and 11.486 years for the reference PV-M. These results show that the PVT-S offers significantly higher economic returns.

6. Future work

In future studies, it would be useful to examine the overall performance of the PVT-S over longer periods and during different seasons, in order to overcome the limitations of tests carried out on a single summer day and to assess its actual annual performance and the most favorable periods for its operation. Additional experimental and numerical investigations could also be conducted to analyze the influence of heat exchanger materials and geometry, as well as local climate variations, with the aim of improving the system's reliability, durability, and long-term performance. Prolonged contact between the heat transfer fluid and the rear surface of the PV-M may also raise issues related to material aging, corrosion, and interface stability, which deserve special attention in future studies. In addition, safety constraints and operational risks associated with long-term operation, such as leaks, hydraulic overpressure, circuit fouling, or degradation of hydraulic components, should be examined to ensure safe and sustainable operation of the system. In addition, the use of alternative fluids, such as nanofluids or phase change materials (PCMs), could be considered to improve thermoelectric performance. Finally, the integration of artificial intelligence-based strategies for managing and optimizing system operation, as well as the joint use of thermal and electrical energy for applications such as green hydrogen production, could offer promising prospects for expanding the functionality and energy efficiency of PVT-S.

CRediT authorship contribution statement

Yassine El Alami: Writing – original draft, Methodology, Investigation, Formal analysis, Data curation, Conceptualization. **Jaouad El Gharfaoui:** Writing – review & editing, Methodology, Formal analysis, Conceptualization. **Zineb Hekss:** Writing – review & editing, Validation, Data curation, Conceptualization. **Charaf Hajjaj:** Writing – review & editing, Validation, Data curation, Conceptualization. **Fatima Chanaa:** Writing – review & editing, Validation, Data curation, Conceptualization. **Elhadi Baghaz:** Writing – review & editing, Validation, Data curation, Conceptualization. **Mohammed Ghazal:** Writing – review & editing, Validation, Funding acquisition, Formal analysis, Conceptualization. **Adnan Ibrahim:** Writing – review & editing, Validation, Supervision, Methodology, Funding acquisition, Formal analysis, Conceptualization.

Declaration of competing interest

The authors declare that they have no known competing financial interests or personal relationships that could have appeared to influence the work reported in this paper.

Data availability

Data will be made available on request.

References

[1] M.M. Ahmed, B.K. Das, P. Das, M.S. Hossain, M.G. Kibria, Energy management and sizing of a stand-alone hybrid renewable energy system for community electricity, fresh water, and cooking gas demands of a remote island, Energy Convers. Manag. 299 (2024) 117865, https://doi.org/10.1016/j.enconman.2023.117865.

[2] Md.G. Kibria, U.K. Paul, A. Hasan, Md.S. Mohtasim, B.K. Das, M. Mourshed, Current prospects and challenges for biomass energy conversion in Bangladesh: attaining sustainable development goals, Biomass Bioenergy 183 (2024) 107139, https://doi.org/10.1016/j.biombioe.2024.107139.

[3] Y. El Alami, A. Ameur, M. Benhmida, A. Rabhi, E. Baghaz, Performance evaluation of different new channel box photovoltaic thermal systems, J. Clean. Prod. 478 (2024) 143953, https://doi.org/10.1016/j.jclepro.2024.143953.

[4] Y. El Alami, E. Baghaz, R. Nasrin, F. Chanaa, R. Bendaoud, S. Padmanaban, M. Louzazni, Experimental-numerical comparative study of performance and cost-effectiveness of partially- and fully-cooled photovoltaic thermal systems, Case Stud, Therm. Eng. 73 (2025) 106660, https://doi.org/10.1016/j.csite.2025.106660.

[5] Y. El Alami, H.E. Achouby, E. Baghaz, C. Hajjaj, R. Nasrin, An innovative photovoltaic thermal system with direct water-cell contact: energy, exergy, and sustainability analysis, Sol. Energy 300 (2025) 113827, https://doi.org/10.1016/j.solener.2025.113827.

[6] Md.S. Mohtasim, U.K. Paul, Md.G. Kibria, B.K. Das, 7E and sustainability analysis of photovoltaic thermal system (PVT) incorporating graphene and Al2O3 nanoparticles with paraffin wax integrated fin arrangements, J. Clean. Prod. 519 (2025) 146007, https://doi.org/10.1016/j.jclepro.2025.146007.

[7] Y.E. Alami, E. Baghaz, R. Nasrin, C. Hajjaj, M. Benhmida, K.M. Al-Aribe, A. Ibrahim, Numerical exploration and relational impact ranking of critical parameters in 3D PV module studies, results eng. (2025) 107097. https://doi.org/10.1016/j.rineng.2025.107097.

[8] P.S. Suman, P. Goyal, Analysing the effects of solar insolation and temperature on PV cell characteristics, Mater, Today Proc. 45 (2021) 5539–5543, https://doi.org/10.1016/j.matpr.2021.02.301.

[9] A. Kazemian, H. Yang, C. Xiang, Assessing the effects of photovoltaic and solar thermal ratios on performance, cost, and emissions in combined solar configurations, Appl. Energy 384 (2025) 125438, https://doi.org/10.1016/j.apenergy.2025.125438.

[10] E.M. Almetwally, A. Khelifa, M.E. Hadi Attia, A.E. Kabeel, M.M. Abdel-Aziz, Boosting PV/T system performance with hybrid ZnO–water nanofluid cooling and passive airflow: a practical insight into the role of nanoparticle concentration, Energy Convers. Manag. 348 (2026) 120595, https://doi.org/10.1016/j.enconman.2025.120595.

[11] A. Kazemian, C. Xiang, Large-scale analysis of photovoltaic, photovoltaic-thermal, and solar thermal systems in high-density urban environments, Appl. Energy 401 (2025) 126765, https://doi.org/10.1016/j.apenergy.2025.126765.

[12] Y. Wang, Z. Quan, Y. Zhao, G. Rosengarten, A. Mojiri, Techno economic analysis of integrating photovoltaic-thermal systems in ground-source heat pumps for heating-dominated regions, Appl. Energy 377 (2025) 124677, https://doi.org/10.1016/j.apenergy.2024.124677.

[13] M. Moein-Jahromi, J. Aboueian, PCM-based annular flow for enhanced thermal management of PV/T units, Energy Convers. Manag. 344 (2025) 120304, https://doi.org/10.1016/j.enconman.2025.120304.

[14] T.T. Göksu, H.F. Öztop, Energy and exergy analysis of perforated twisted tapes: rSM-driven optimization of geometrical parameters for PV/T systems, Appl. Therm. Eng. 279 (2025) 127550, https://doi.org/10.1016/j.applthermaleng.2025.127550.

[15] M.I.A. Zaini, M. Mustapha, N.S. Nazri, N.N. Rosli, M.A. Mutalib, W.M.W. Sulong, M.A. Ibrahim, A. Fudholi, Innovative water-cooling system for enhanced energy efficiency in photovoltaic-thermal system, Case Stud, Therm. Eng. 70 (2025) 106137, https://doi.org/10.1016/j.csite.2025.106137.

[16] B.O. Ahmed, A. Ibrahim, H.L. Azeez, M. Jaber, A.H.A. Al-Waeli, H. Jarimi, 4E Investigation of a solar collector design featuring ribs, petals, and helical twisted tapes in a photovoltaic thermal system, Arab, J. Sci. Eng. 50 (2025) 18905–18924, https://doi.org/10.1007/s13369-025-09962-6.

[17] K. Parach, B. Jafari, K. Hosseinzadeh, Numerical analysis of integrated photovoltaic thermal systems utilizing nanoparticles with phase change material and fin attachments, Int. J. Thermofluids 27 (2025) 101210, https://doi.org/10.1016/j.ijft.2025.101210.

[18] F. Beltrán, N. Sommerfeldt, C. Reichl, H. Madani, Cold solar: PVT heat exchanger designs for heat pump integration, Appl. Therm. Eng. 261 (2025) 125020, https://doi.org/10.1016/j.applthermaleng.2024.125020.

[19] A.M.O. Al-Karboly, A. Ibrahim, A. Fazlizan, K. Sopian, A.B. Al-Aasam, M.A.A. B. Ishak, A.H.A. Al-Waeli, M. Elmnifi, Experimental evaluation of a photovoltaic thermal collector using twisted tape absorber with nano-enhanced phase change material for thermal storage, J. Energy Storage 109 (2025) 115122, https://doi.org/10.1016/j.est.2024.115122.

[20] T. Wei, X. Wu, T. Zhang, S. Cao, Z. Gu, X. Luo, Efficacy of absorber-plateless PV/T system: with low-cost and energy-efficient plastic capillary exchanger, Appl. Therm. Eng. 273 (2025) 126544, https://doi.org/10.1016/j.applthermaleng.2025.126544.

[21] A. Perwez, D. Li, N.J. Piaget, G. Qin, X. Zheng, Thermal and electrical enhancement of PV/T system using dimpled/protruded channels, Energy 327 (2025) 136454, https://doi.org/10.1016/j.energy.2025.136454.

[22] P. Jha, B. Das, R. Gupta, N. Kumar, An experimental analysis of photovoltaic thermal collector with trapezoidal and plain plates: an energy, exergy, and life cycle assessment, Appl. Therm. Eng. 274 (2025) 126769, https://doi.org/10.1016/j.applthermaleng.2025.126769.

[23] M.A. Alnakeeb, M.A. Abdel Salam, M.A. Hassab, W.M. El-Maghlany, Influence of trapezoidal tube parameters on electrical and thermal performance of hybrid photovoltaic solar panels integrated with phase change materials, Case Stud, Therm. Eng. 65 (2025) 105641, https://doi.org/10.1016/j.csite.2024.105641.

[24] H. Raad, S. Ali, J. Faraj, C. Castelain, K. Chahine, M. Khaled, Enhancing photovoltaic panel efficiency through water-cooling: a parametric comparative evaluation of energetic, economic, and environmental benefits, Unconv. Resour. 7 (2025) 100208, https://doi.org/10.1016/j.uncres.2025.100208.

[25] M.M. Maseer, F.B. Ismail, H.A. Kazem, D.M. Hachim, K.A.H. Al-Gburi, M. T. Chaichan, Performance enhancement of photovoltaic/thermal collector semicircle absorber tubes using nanofluid and NPCM, Renew. Energy 233 (2024) 121152, https://doi.org/10.1016/j.renene.2024.121152.

[26] M.F. Umam, M. Hasanuzzaman, N.Abd Rahim, Experimental investigation and performance evaluation of spiral and serpentine collectors based photovoltaic thermal system in Peninsular Malaysia, Sustain. Energy Technol. Assess. 58 (2023) 103373, https://doi.org/10.1016/j.seta.2023.103373.

[27] Sachit, F.A., Rosli, M.A.M., Tamaldin, N., Misha, S., Abdullah, A.L., Modelling, validation and analyzing performance of Serpentine-direct PV/T solar collector design, (2019).

[28] D. Zhang, Y. Zhou, Z. Yu, T. Ma, X. Wang, Experimental study on electricity generation performance of T-type direct-expansion solar PVT heat pump system, Eng. Rep. 6 (2024) e13013, https://doi.org/10.1002/eng2.13013.

[29] F.A. Radhi, A. Ibrahim, H.L. Azeez, A. Fazlizan, K. Sopian, A.A. Ali, A.B. Al-Aasam, Experimental analysis of a photovoltaic thermal collector utilizing a novel spring insert in a micro-fin absorber tube with twisted tape, nanofluid, and nanophase change material integration, Appl. Therm. Eng. 269 (2025) 126128, https://doi.org/10.1016/j.applthermaleng.2025.126128.

[30] H.A. Kazem, A.H.A. Al-Waeli, M.T. Chaichan, K.H. Al-Waeli, A.B. Al-Aasam, K. Sopian, Evaluation and comparison of different flow configurations PVT systems in Oman: a numerical and experimental investigation, Sol. Energy 208 (2020) 58–88, https://doi.org/10.1016/j.solener.2020.07.078.

[31] S. Aghakhani, M. Afrand, A. Karimipour, R. Kalbasi, M.M. Razzaghi, Numerical study of the cooling effect of a PVT on its thermal and electrical efficiency using a Cu tube of different diameters and lengths, Sustain. Energy Technol. Assess. 52 (2022) 102044, https://doi.org/10.1016/j.seta.2022.102044.

[32] A. Shahsavar, Experimental evaluation of energy and exergy performance of a nanofluid-based photovoltaic/thermal system equipped with a sheet-and-sinusoidal serpentine tube collector, J. Clean. Prod. 287 (2021) 125064, https://doi.org/10.1016/j.jclepro.2020.125064.
[33] S. Ali, P. Kalita, B.J. Bora, M.J. Deka, P. Kalita, P.P. Dutta, Two novel dual-tube photovoltaic-thermal collector designs with improved performance for liquid-cooled photovoltaic-thermal systems, Renew. Energy 232 (2024) 121062, https://doi.org/10.1016/j.renene.2024.121062.
[34] M. Madadi, A.A. Abbasian Arani, Experimental evaluation of photovoltaic thermal (PVT) system using a modular heat collector with flat back shape fins, pipe, nanofluids and phase change material, Sol. Energy Mater. Sol. Cells 280 (2025) 113294, https://doi.org/10.1016/j.solmat.2024.113294.
[35] A. Alqatamin, S. Jinzhan, Numerical analysis and design of photovoltaic-thermal (PVT) system with novel water-cooling channel structure integrated with perforated V-shape fins, Renew. Energy 243 (2025) 122587, https://doi.org/10.1016/j.renene.2025.122587.
[36] C. Yu, H. Li, J. Chen, S. Qiu, F. Yao, X. Liu, Investigation of the thermal performance enhancement of a photovoltaic thermal (PV/T) collector with periodically grooved channels, J. Energy Storage 40 (2021) 102792, https://doi.org/10.1016/j.est.2021.102792.
[37] R. Nasrin, N.A. Rahim, H. Fayaz, M. Hasanuzzaman, Water/MWCNT nanofluid based cooling system of PVT: experimental and numerical research, Renew. Energy 121 (2018) 286–300, https://doi.org/10.1016/j.renene.2018.01.014.
[38] Y. Zhang, Y. Zhao, H. Zhang, C. Cheng, D. Gao, H. Chen, J. Liu, Numerical optimization and performance study of a photovoltaic/thermal module based on multi-stage V-type turbulators, Renew. Energy 252 (2025) 123559, https://doi.org/10.1016/j.renene.2025.123559.
[39] J. Satpute, C. Srinidhi, S.S. Rathore, S.M. Yadav, A. Kumar, A. Gajbhiye, S. V. Channapattana, K. Aithal, Parametric influence and efficiency assessment of water-cooled photovoltaic thermal PV/T absorber designs, Energy 320 (2025) 135218, https://doi.org/10.1016/j.energy.2025.135218.
[40] M.S. Hossain, A.K. Pandey, J. Selvaraj, N. Abd Rahim, A. Rivai, V.V. Tyagi, Thermal performance analysis of parallel serpentine flow based photovoltaic/thermal (PV/T) system under composite climate of Malaysia, Appl. Therm. Eng. 153 (2019) 861–871, https://doi.org/10.1016/j.applthermaleng.2019.01.007.
[41] S. Hosouli, S. Bagde, M. Talha Jahangir, S. Hasnain Qamar, N. Formosa, J. Gomes, Mitigating PV cell cracking in solar photovoltaic thermal collectors with a novel H-pattern absorber design, Appl. Therm. Eng. 242 (2024) 122516, https://doi.org/10.1016/j.applthermaleng.2024.122516.
[42] Y. Zhang, C. Shen, C. Zhang, G. Lv, C. Sun, D. Chwieduk, The study of heat control on PVT modules with a new leaf-like heat exchanger, J. Renew. Sustain. Energy 13 (2021) 023703, https://doi.org/10.1063/5.0030541.
[43] M.G. Ajel, E. Gedik, H.A. Abdul Wahhab, B.A. Shallal, Performance analysis of an open-flow photovoltaic/thermal (PV/T) solar collector with using a different fins shapes, Sustainability 15 (2023) 3877, https://doi.org/10.3390/su15053877.
[44] K. Sopian, G.L. Jin, M.Y. Othman, S.H. Zaidi, M. Hafidz, Advanced absorber design for photovoltaic thermal (PV /T) collectors, Recent Res. Energy, Environ. Landsc. Archit. 978-1–6180 (2011) 77–83, n.d.
[45] K.S. J, Describing uncertainties in single-sample experiments, Mech Eng 75 (1963) 3–8.
[46] U. Olmuş, Y.E. Güzelel, K.N. Çerçi, O. Büyükalaca, Numerical analysis and comparison of different serpentine-based photovoltaic-thermal collectors, Renew. Energy 241 (2025) 122196, https://doi.org/10.1016/j.renene.2024.122196.
[47] Y.E. Alami, B. Zohal, R. Bendaoud, M. Rhiat, A. Rabhi, B. Benhala, K. Hirech, E. Baghaz, Comparative analysis of the performance of Shingle and Standard photovoltaic technologies in the environmental conditions of El Jadida, E3S Web Conf. 601 (2025) 00010, https://doi.org/10.1051/e3sconf/202560100010.
[48] Y. El Alami, E. Baghaz, M. Errebii, R. Nasrin, M.E.H. Amagour, K.M. Al-Aribe, A. Ibrahim, Numerical perspective of copper nanoparticle morphology on energy conversion in a novel photovoltaic-thermal system, Energy 342 (2026) 139598, https://doi.org/10.1016/j.energy.2025.139598.
[49] Y.E. Alami, F. Ouerradi, S. Bounouar, M. Benhmida, M. Rhiat, B. Benhala, K. Hirech, E. Baghaz, Comparative study of the performance of photovoltaic and photovoltaic thermal solar systems: case study in El Jadida, E3S Web Conf. 601 (2025) 00011, https://doi.org/10.1051/e3sconf/202560100011.
[50] Y. El Alami, E. Baghaz, R. Bendaoud, R. Nasrin, Pressure drops reduction and performance optimization strategies of an innovative channel box photovoltaic thermal system, Int. J. Photoenergy 2025 (2025) 8744508, https://doi.org/10.1155/ijph/8744508.
[51] S. Abbas, J. Zhou, A. Hassan, Y. Yuan, S. Yousuf, Y. Sun, C. Zeng, Economic evaluation and annual performance analysis of a novel series-coupled PV/T and solar TC with solar direct expansion heat pump system: an experimental and numerical study, Renew. Energy 204 (2023) 400–420, https://doi.org/10.1016/j.renene.2023.01.032.
[52] R.K. Rajamony, A.K. Pandey, A.G.N. Sofiah, M.A. Wadaan, J.K. Siaw Paw, S. K. Suraparaju, A. Baabbad, M. Samykano, V. Paranthaman, Energy, exergy, economic and environmental (4E) analysis of serpentine tube absorber photovoltaic thermal system using nano enhanced phase change material, Energy 319 (2025) 135032, https://doi.org/10.1016/j.energy.2025.135032.
[53] M. Alktranee, Q. Al-Yasiri, M.A. Shehab, P. Bencs, Z. Németh, K. Hernadi, Experimental and numerical study of a photovoltaic/thermal system cooled by metal oxide nanofluids, Alex. Eng. J. 94 (2024) 55–67, https://doi.org/10.1016/j.aej.2024.03.050.
[54] H.L. Azeez, A. Ibrahim, B.O. Ahmed, S.S. Dol, A.H.A. Al-Waeli, M. Jaber, Experimental investigations of heat transfer, energy, and exergy-based sustainability of a novel photovoltaic thermal system, Case Stud, Therm. Eng. 70 (2025) 106089, https://doi.org/10.1016/j.csite.2025.106089.
[55] M. Zohri, Suwarno Prabowo, E. Solomin, M.H. Yazdi, T. Suyono, H. Abimanyu, A. Fudholi, Sustainability index and a bibliometric of photovoltaic thermal with rectangular channel, Case Stud, Therm. Eng. 63 (2024) 105300, https://doi.org/10.1016/j.csite.2024.105300.
[56] H.L. Azeez, A. Ibrahim, B.O. Ahmed, J. Kasprzak, A.H.A. Al-Waeli, M. Jaber, 5E assessments of a novel solar collector under high cooling demand scenarios: experimental and sustainability studies, Energy 326 (2025) 136297, https://doi.org/10.1016/j.energy.2025.136297.
[57] Y.E. Alami, E. Baghaz, R. Nasrin, S. Padmanaban, M. Louzazni, Numerical approach of an advanced hybrid photovoltaic thermal system based on exergy, energy, enviro-economic, and sustainability factors, Results Eng 27 (2025) 106342, https://doi.org/10.1016/j.rineng.2025.106342.
[58] Y.E. Alami, E. Baghaz, R. Nasrin, K. Haboubi, M. Benhmida, A. Ibrahim, Integrated sustainability and 4E analysis of hybrid nanofluid featured PVT systems incorporating diverse backsheets, Appl. Therm. Eng. 284 (2026) 129147, https://doi.org/10.1016/j.applthermaleng.2025.129147.
[59] A.M. Ramezani, A.M. Jadidi, S. Rashidi, Techno-economic and environmental investigation between a low-concentrating photovoltaic thermal collector and a regular photovoltaic flat plate thermal collector, Int. Commun. Heat Mass Transf. 155 (2024) 107529, https://doi.org/10.1016/j.icheatmasstransfer.2024.107529.
[60] Y. El Alami, M. Rami, C. Hajjaj, M. Benhmida, A. Faize, E. Baghaz, Three-dimensional thermal modeling and analysis of the heat source, the impact of encapsulation materials and the back sheet of silicon PV modules, Appl. Therm. Eng. 280 (2025) 128430, https://doi.org/10.1016/j.applthermaleng.2025.128430.
[61] Y.E. Alami, H. Dahmani, F. Ouerradi, B. Zohal, R. Bendaoud, E. Baghaz, Impact of heat exchanger materials on the performance of Solar hybrid photovoltaic Thermal (PVT) systems: 3D analysis, Eds, in: B. Hajji, A. Gagliano, A. Mellit, A. Rabhi, M. Calì (Eds.), Proc. 4th Int. Conf. Electron. Eng. Renew. Energy Syst. 2, Springer Nature, Singapore, 2025, pp. 609–619, https://doi.org/10.1007/978-981-97-9975-6_58. -.
[62] Y. El Alami, E. Baghaz, R. Bendaoud, F. Chanaa, M. Benhmida, H. Ezzaki, R. Nasrin, Experimental-numerical investigation of the photovoltaic Thermal system with polypropylene heat exchanger: case in Morocco, IET Renew. Power Gener. 19 (2025) e70041, https://doi.org/10.1049/rpg2.70041.
[63] A. Nahar, M. Hasanuzzaman, N.A. Rahim, Numerical and experimental investigation on the performance of a photovoltaic thermal collector with parallel plate flow channel under different operating conditions in Malaysia, Sol. Energy 144 (2017) 517–528, https://doi.org/10.1016/j.solener.2017.01.041.
[64] E. Bisengimana, J. Zhou, M. Binama, Y. Yuan, Numerical investigation on the factors influencing the temperature distribution of photovoltaic/thermal (PVT) evaporator/condenser for heat pump systems, Renew. Energy 194 (2022) 885–901, https://doi.org/10.1016/j.renene.2022.05.154.
[65] M. Ahmadinejad, A. Soleimani, A. Gerami, The effects of a novel baffle-based collector on the performance of a photovoltaic/thermal system using SWCNT/Water nanofluid, Therm. Sci. Eng. Prog. 34 (2022) 101443, https://doi.org/10.1016/j.tsep.2022.101443.
[66] A. Kazemian, A. Salari, T. Ma, A year-round study of a photovoltaic thermal system integrated with phase change material in Shanghai using transient model, Energy Convers. Manag. 210 (2020) 112657, https://doi.org/10.1016/j.enconman.2020.112657.
[67] A. Kazemian, A. Salari, A. Hakkaki-Fard, T. Ma, Numerical investigation and parametric analysis of a photovoltaic thermal system integrated with phase change material, Appl. Energy 238 (2019) 734–746, https://doi.org/10.1016/j.apenergy.2019.01.103.
[68] Météo Blue, meteoblue. https://www.meteoblue.com/fr/meteo/semaine/blue_%c3%89tats-unis_5286039, 2026 accessed February 4, 2026.
[69] A. Shahsavar, Experimental evaluation of energy and exergy performance of a nanofluid-based photovoltaic/thermal system equipped with a sheet-and-sinusoidal serpentine tube collector, J. Clean. Prod. 287 (2021) 125064, https://doi.org/10.1016/j.jclepro.2020.125064.
[70] H. Atalay, C. Tunçkal, S. Türkdoğan, M. Direk, Exergetic, sustainability and exergoeconomic analyses of a fully photovoltaic-powered heat pump tumble dryer, Renew. Energy 225 (2024) 120274, https://doi.org/10.1016/j.renene.2024.120274.
[71] S. Bestas, I.S. Aktas, F. Bayrak, A bibliometric and performance evaluation of nano-PCM-integrated photovoltaic panels: energy, exergy, environmental and sustainability perspectives, Renew. Energy 226 (2024) 120383, https://doi.org/10.1016/j.renene.2024.120383.
[72] M. Zohri, W. Ramadhan, A. Fudholi, Improvement potential and sustainability index of photovoltaic thermal solar air collector, Int. J. Heat Technol. 40 (2022) 743–748, https://doi.org/10.18280/ijht.400312.
[73] M. Zohri, Suwarno Prabowo, E. Solomin, M.H. Yazdi, T. Suyono, H. Abimanyu, A. Fudholi, Sustainability index and a bibliometric of photovoltaic thermal with rectangular channel, Case Stud, Therm. Eng. 63 (2024) 105300, https://doi.org/10.1016/j.csite.2024.105300.
[74] M. Zohri Yuliadi, M. Ghazali Idham, Performance of photovoltaic thermal technology using V-absorber with exergy, improvement potential and sustainability index analysis, Math. Model. Eng. Probl. 10 (2023) 551–557, https://doi.org/10.18280/mmep.100223.
[75] P. Rajput, G.N. Tiwari, O.S. Sastry, Thermal modelling with experimental validation and economic analysis of mono crystalline silicon photovoltaic module on the basis of degradation study, Energy 120 (2017) 731–739, https://doi.org/10.1016/j.energy.2016.11.123.

[76] E.M. Abo-Zahhad, A.A. Hachicha, A. Radwan, Z. Said, S.M.A. Rahman, S. Haridy, Comprehensive performance evaluation of new photovoltaic/serpentine collectors using response surface methodology: energy, exergy, and environmental perspectives, Sol. Energy 268 (2024) 112258, https://doi.org/10.1016/j.solener.2023.112258.

[77] C.S. Rajoria, S. Agrawal, G.N. Tiwari, Exergetic and enviroeconomic analysis of novel hybrid PVT array, Sol. Energy 88 (2013) 110–119, https://doi.org/10.1016/j.solener.2012.11.018.

[78] O. Büyükalaca, H.M. Kılıç, U. Olmuş, Y.E. Güzelel, K.N. Çerçi, Numerical investigation and ANN modeling of performance for hexagonal boron nitride-water nanofluid PVT collectors, Therm. Sci. Eng. Prog. 43 (2023) 101997, https://doi.org/10.1016/j.tsep.2023.101997.

[79] M. El Hadi Attia, M.E. Zayed, A.E. Kabeel, A. Khelifa, K. Irshad, S. Rehman, Numerical analysis and design of a novel solar photovoltaic thermal system using finned cooling channel structures embedded with air/TiO2–water nano bi-fluid, Sol. Energy 269 (2024) 112368, https://doi.org/10.1016/j.solener.2024.112368.

[80] Z.M. Mahdi, A.N. Al-Shamani, A. Al-Manea, H.A. Al-zurfi, R. Al-Rbaihat, K. Sopian, A. Alahmer, Enhancing photovoltaic thermal (PVT) performance with hybrid solar collector using phase change material, porous media, and nanofluid, Sol. Energy 283 (2024) 112983, https://doi.org/10.1016/j.solener.2024.112983.

[81] T. Maatallah, R. Zachariah, F.G. Al-Amri, Exergo-economic analysis of a serpentine flow type water based photovoltaic thermal system with phase change material (PVT-PCM/water), Sol. Energy 193 (2019) 195–204, https://doi.org/10.1016/j.solener.2019.09.063.

[82] S. Sreekumar, A. Pugsley, S. Chakrabarti, N. Hewitt, J.D. Mondol, N. Shah, Experimental investigation on the performance of MXene/C-dot hybrid nanofluid-based photovoltaic/thermal system: an energy, Exergy, and Enviro-economic analysis, Sol. Energy Mater. Sol. Cells 272 (2024) 112904, https://doi.org/10.1016/j.solmat.2024.112904.

[83] M. Abd El-Hamid, G. Wei, Effect of varying the thermophysical properties of phase change material on the performance of photovoltaic/thermal-PCM hybrid module numerically, J. Energy Storage 86 (2024) 111326, https://doi.org/10.1016/j.est.2024.111326.

[84] C. Ould-Lahoucine, H. Ramdani, D. Zied, Energy and exergy performances of a TiO2-water nanofluid-based hybrid photovoltaic/thermal collector and a proposed new method to determine the optimal height of the rectangular cooling channel, Sol. Energy 221 (2021) 292–306, https://doi.org/10.1016/j.solener.2021.04.027.

[85] T. Alsharifi, J.M. Mahdi, H. Togun, H.M. Taqi Al-Najjar, N. Ben Khedher, A. Cairns, P. Talebizadehsardari, Design and optimization of a household photovoltaic/thermal collector with serpentine tube: energy and exergy analysis, Appl. Therm. Eng. 246 (2024) 122983, https://doi.org/10.1016/j.applthermaleng.2024.122983.

[86] S. Aberoumand, S. Ghamari, B. Shabani, Energy and exergy analysis of a photovoltaic thermal (PV/T) system using nanofluids: an experimental study, Sol. Energy 165 (2018) 167–177, https://doi.org/10.1016/j.solener.2018.03.028.

[87] T.T. Göksu, H.F. Öztop, Energy and exergy analysis of perforated twisted tapes: rSM-driven optimization of geometrical parameters for PV/T systems, Appl. Therm. Eng. 279 (2025) 127550, https://doi.org/10.1016/j.applthermaleng.2025.127550.